UNIVERSITY OF OKLAHOMA

GRADUATE COLLEGE

SULFOXIDE SURFACTANTS

A DISSERTATION

SUBMITTED TO THE GRADUATE FACULTY

in partial fulfillment of the requirements for the

Degree of

DOCTOR OF PHILOSOPHY

By

ZAHRA SHAHRASHOOB
Norman, Oklahoma
2018

SULFOXIDE SURFACTANTS

A DISSERTATION APPROVED FOR THE
SCHOOL OF CHEMICAL, BIOLOGICAL AND MATERIALS
ENGINEERING

BY

_____
Dr. Brian Grady, Chair

_____
Dr. David Sabatini

_____
Dr. Steven Crossley

_____
Dr. Jeffrey Harwell

_____
Dr. Edgar O Rear

Acknowledgements

Many thanks to my advisor Dr. Brian Grady, who supported my decisions and provided me the opportunity to teach a class on the path of my doctoral degree. I sincerely appreciate his patience. Thanks also to my committee members Dr. Steven Crossley, Dr. Jeffrey Harwell, Dr. Edgar O'Rear and Dr. David Sabatini.

This project was sponsored by Novus International. Thanks to Scott Long and Dr. Graciela Arhancet for their close collaboration and help.

I would also like to acknowledge the following people: Kevin Carr, Changlong Chen, Terri Colliver, Joshua Jacob Hamon, Fatoumata Ide Seyni, Alan Miles, Mesude Ozturk and Shengbo Wang.

I would like to thank my family who provided me with encouragement, support and love.

Last but not least is my fiancé Akbar. This PhD belongs to him.

Table of Contents

List of Tables

List of Figures

Abstract

A novel group of nonionic surfactants, which we term ester sulfoxides, derived from 2-hydroxy-4-(methylthio) butyric acid are characterized in this thesis. The physico-chemical properties, equilibrium and dynamic properties, and microemulsion behavior of these surfactants are investigated. Based on the physico-chemical properties, the sulfoxide nonionic surfactant molecules presented good surface activity, good foaming, wetting ability and laundry detergency performance. Equilibrium surface tensions were determined for a number of molecules. The Langmuir adsorption isotherm is satisfactory for describing the adsorption behavior of the sulfoxide surfactant at the air/water interface. Adsorption kinetics onto the air/water interface was studied for an ester sulfoxide molecule with 8 carbon atoms in the tail of the surfactant. Comparing the experimental dynamic surface tension profiles of the surfactant solutions with the diffusion-controlled kinetic model indicate that the adsorption of this surfactant molecule onto the air/water interface is diffusion-controlled for dilute solutions at 25°C. HLD parameters of longer-chain surfactants were obtained and compared to that of alcohol ethoxylates. Ester sulfoxides are much less temperature sensitive than alcohol ethoxylates, and have a temperature coefficient similar to that of ionic surfactants. The ester sulfoxide moiety was determined to be as hydrophilic as ~5 ethylene oxide units according to the Cc value of the HLD parameters.

1. Introduction

1.1 Surfactants, structures and properties

Surfactants are surface active molecules. They are molecules consisting of hydrophilic moiety (polar groups) referred to as the head attached to a hydrophobic moiety (nonpolar groups) referred to as the tail of the surfactant [1].

The tail groups are usually hydrocarbon chains which may be straight or branched chain, saturated or unsaturated. Aromatic groups may also be present in the hydrocarbon tail. Other than the hydrocarbon surfactants there are also silicone-based and fluorocarbon chains as well.

The head groups could be anions including sulfonate, carboxylate, and phosphate or could be cations. These cation head groups are mostly based on amines including primary, secondary, tertiary and quaternary ammonium. The head group of the surfactants could also be nonionic groups including esters, amides, ethers, polyoxyethylene and polyoxypropylene. There are another type of the surfactant head groups called zwitterionics; these molecules have both positive and negative headgroups, which dominates depends on pH. Among this groups are the amino acids and the derivatives, amine oxides etc.

Water resists the incorporation of the hydrophobic hydrocarbon tail into its structure. The hydrophilic or polar part, in contrast likes water and remains in the

water. Hence when the surfactants are added to the water there are two favorable configurations, not including the case where free surfactant is dissolved in the water.

One favorable configuration is that the tail group of the surfactant is removed from the water and the head group remains in the water. This is achieved by the adsorption of a monolayer of the surfactants at the interface between water and air and hence reduces the surface tension between the air/water interface [1].

The second favorable configuration is micellization. Above a threshold surfactant concentration, called the critical micelle concentration (cmc), the surfactant molecules self-assemble into aggregates known as micelles. The hydrophobic tails partly shield themselves from water in the aggregate interior and the hydrophilic heads expose themselves to the water at the aggregate or micelle surface [1]. Figure 1.1 shows an adsorption monolayer and the micelle formation in surfactant solutions.

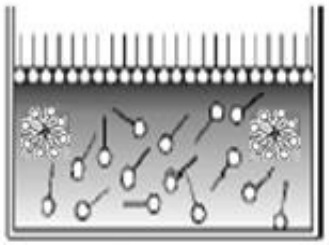

Figure 1. 1. Adsorption layer at the air/water interface and micelle formation in surfactant solution

1.2 Literature review

1.2.1 Sulfoxide surfactants

Surfactants containing sulfoxide functional groups have not been broadly studied. These surfactants were described in the mid-20th century in several patents [2-5]. U.S. patent, issued April 1957 [4] disclosed sulfoxides of the formula RSOR' as detergent surfactants which were said to clean synergistically when combined with other surfactants. Later in 1969, French patent [5] described alkylethoxylate sulfoxides as detergent surfactants especially effective in cold water. Hennaux and Laschewsky reported a new group of polymerizable sulfoxide containing surfactants. The polymerization is not based on the hydrophilic groups, but rather the double bonds in the hydrophobe [6,7] A few studies were done to understand the properties of sulfoxide containing surfactants. Clint and Walker studied the behavior of sulfoxide surfactants in homologous and mixed micelles [8,9]. Mixing behavior of sulfoxide-containing surfactants were explored with different hydrophobe sizes [10], with other nonionic surfactants [11,12] and with other ionic surfactants [13,14], or with salts [15-19]. Iyota et al. found that the adsorption change of alkyl sulfoxide surfactants with salinity resembles nonionic surfactants more than ionic surfactants [17,18].

The surfactants characterized in this thesis contain a linear hydrocarbon in the tail group and ester sulfoxide in the head group. The current work marks the first time that esters were used along with sulfoxide groups in a single surfactant molecule.

These surfactants were synthesized by the Novus International. The synthesis process is composed of two reactions: esterification of fatty alcohol with 2-hydroxy-4-(methylthio) butyric acid (HMTBA); and partial oxidation of the sulfide to a sulfoxide using hydrogen peroxide. The oxidation step significantly increase the molecule's water solubility. Structures are shown in Figure 1.2.

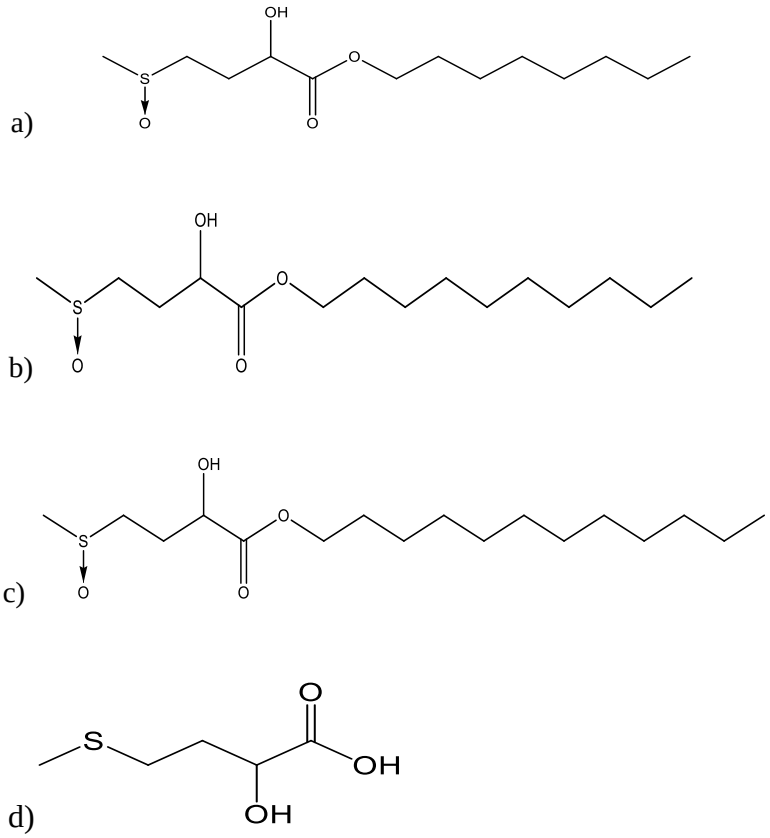

Figure 1. 2. a) octyl 2-hydroxy-4-(methylsulfinyl)butanoate, C_8ESO, b) decyl 2-hydroxy-4-(methylsulfinyl) butanoate, C_{10}ESO, c) dodecyl 2-hydroxy-4-(methylsulfinyl), C_{12}ESO and d) 2-hydroxy4-(methylthio) butyric acid, HMTBA

In this study we investigate the fundamental surfactancy of ester sulfoxides in water-surfactant systems. First the structures of various molecules based on these synthetic steps are characterized by ^{1}H NMR. Then the phase behavior of the sulfoxide surfactants in water solutions is studied. The calcium tolerance of these surfactants is investigated, to understand the nature of the head group charge type. Other surfactant properties, such as CMC, surface tension at CMC (γ_{CMC}), cloud temperature, adsorption at liquid/solid, Draves wetting kinetics, Ross-Miles foaming ability, foam collapse profile and laundry performance as nonionic surfactant in an enzyme and brightener containing liquid formulation are investigated and compared to other surfactants.

1.2.2 Dynamic surface tension (DST)

When a surface forms in a surfactant solution, equilibrium between volume and surface concentration only occurs after a certain amount of time, as the surface active molecules need time to move or diffuse to the surface and to adsorb on to the surface. This results in a time-dependent surface tension characteristic or dynamic surface tension (DST).

A freshly formed interface of a surfactant solution has a surface tension, γ, very close to that of the solvent, $\gamma_{0.}$ Over a period of time, γ will decay to the equilibrium value γ_{eq}, and this period of time can range from milliseconds to days depending on the surfactant type and concentration [20].

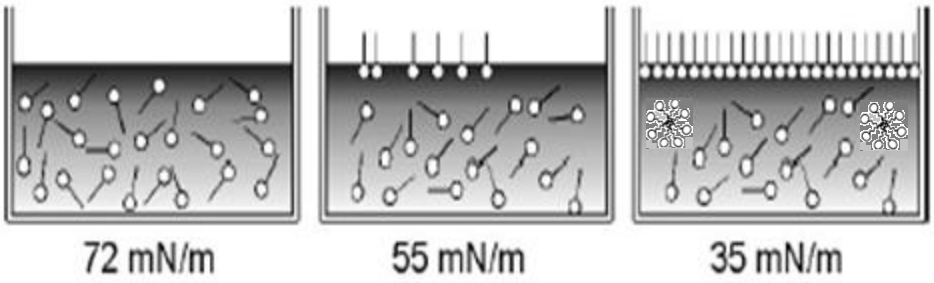

Figure 1. 3. Adsorption of the surfactant into the freshly formed surface

Surface concentrations are not easily measured directly in experiments and hence surface tension is a more common measure for detecting adsorption. Dynamic surface tension, $\gamma(t)$, is an important property and it governs important industrial processes [20]. For example in the photographic industry the formulation of thin gelatin films requires high flow velocities. The dynamic surface tension in fast time scales (<1s) affects the stress which control the flow. DST affects the dynamical wettability in coating processes. Film retraction or crawling can be minimized by controlling the dynamic surface tensions in emulsions. DST is also important in agrochemicals where easy spreading of pesticides onto leaves requires fast wettability [21]. One biological process where the control of DST is essential is during the inhalation and exhalation in the lung, where the control of the DST by pulmonary surfactants is necessary for effective functioning of the alveoli [22]. Another example is the rapid water wetting of fabric for surface treatment, dyeing or resin impregnation. DST is important in emulsifiers, wetting and foaming agents [23], cosmetics [24], foods and bioprocessing [25], petroleum industry [26], metal, paper and textiles industries [27-29].

The goal in the above applications is to select surfactants that will effectively reduce the surface tension to a desired value within a desired time. An optimum use of the surfactants in these applications is possible only with an insight into transport and dynamic surface tension properties of surfactants along with their equilibrium properties.

1.2.2.1 Experimental methods for determining dynamic surface tension

A broad time interval needs to be studied in order to fully characterize the time dependence of surface tension for various surfactant concentrations. Multiple experiments are necessary to cover the time range from less than a millisecond up to minutes, hours and even days.

Table 1.1 summarizes the most frequently used surface tension methods, their available time and temperature intervals [20].

Table 1. 1. Surface tension methods [20]

Method	Suitability for liquid/gas interface	Typical Available range	Typical Temperature range
Capillary rise	Good	10s - 24h	20-25 °C
Drop volume	Good	1s – 1000s	10-90 °C
Growing drop/bubble	Good	0.01s - 600s	10-90 °C
Inclined plate	Good	0.1s - 10s	20-25 °C

Maximum bubble pressure	Good	0.1ms - 200s	10-90 °C
Oscillating jet	Good	0.001s - 0.02s	20- 25 °C
Drop Shape Analyzer	Good	5s - 24h	20-90 °C
Plate tensiometer	Good	10s -24h	20-45 °C
Ring tensiometer	Good	30s - 24h	20-45 °C
Spinning drop	Possible	Instant	10-90 °C
Static drop volume	Good	10s - 1000s	10-90 °C
Capillary waves	Possible	0.001s - 0.1s	20-25 °C
Elastic ring	Good	10s - 24h	20-25 °C

1.2.2.2 Equilibrium adsorption isotherms and surface equation of state

When surfactant molecules adsorb from an aqueous solution onto the air/water interface, adsorption proceeds until an equilibrium is reached. This thermodynamic equilibrium is established when the chemical potentials of the surfactant at the interface and in the bulk are equal. The chemical potential of surfactant molecules at the interface can be described as a function of the surfactant surface concentration Γ. Γ is the amount of surfactant at the interface per unit area. The relationship between the bulk concentration and surface concentration at a constant temperature is the equilibrium adsorption isotherm, $\Gamma(C)$. The relationship between the surface tension and surface concentration is the surface equation of state, $\gamma(\Gamma)$.

A classical equation which relates the surface tension, surface concentration and bulk concentration is the Gibbs equation [1].

$$\Gamma = -\frac{1}{nRT}\left(\frac{\partial \gamma}{\partial\, lnC}\right)_T \qquad (1.1)$$

Where R is the gas constant and T is the temperature. The factor n is a constant which depends on the number of species constituting the surfactant and adsorbing at the interface. For a non-ionic surfactant, n = 1. For an ionic surfactant in the absence of supporting electrolyte, n = 2 is used. [1] With the Gibbs equation and a proper isotherm $\Gamma(C)$, one can derive a corresponding surface equation of state $\gamma(\Gamma)$, and then find $\gamma(C)$.

The commonly used method to find the adsorption isotherm and surface equation of state is as follows [30]. First an analytical form of the adsorption isotherm with the unknown parameters of the isotherm is assumed. Second the adsorption isotherm is substituted into the Gibbs equation and the resultant equation integrated to obtain a surface equation of state and an expression for the $\gamma(C)$ relationship. Third, $\gamma(C)$ is fitted to the experimentally measured data to find the unknown parameters of the isotherm. When the parameters are known the adsorption isotherm and surface equation of state are established. Numerous studies have been done to find the surfactant equilibrium properties. [30-35].

1.2.2.3 Adsorption isotherms

In this section we review some surfactant equation of state and adsorption isotherms.

For single-component systems, the simplest isotherm is the Henry isotherm:

$$\Gamma = K_H C \qquad (1.2)$$

The equilibrium adsorption constant $K_{H,}$ has dimensions of length, is a measure of the surface activity of a surfactant.

The most commonly used non-linear isotherm is the Langmuir isotherm:

$$\Gamma = \Gamma_m \frac{K_L C}{1 + K_L C} \qquad (1.3)$$

Where Γ_m is the maximum surface concentration and K_L is the Langmuir equilibrium adsorption constant. From the maximum slope of $d\gamma/d\ln C$ at concentrations near the cmc, one can only obtain a maximum surface concentration, Γ_m [1].

At low concentrations, or when $K_L c \ll 1$, the Langmuir isotherm can be approximated by the Henry isotherm:

$$K_H = \Gamma_m K_L \qquad (1.4)$$

The value of K_L and K_H provides a useful measure of the surfactant activity. For example from Table 1.2 it can be seen that Triton X-100 is the most surface active

surfactant with the K_L of $1.5*10^3 m^3/mol$. The Langmuir equation accounts for a lattice-type model of the surface molecules. In this model it is assumed that surface molecules do not interact with each other.

The Frumkin isotherm, considers solute-solvent interactions at a non-ideal surface. It has also been used for several systems. [36-45].

$$C = \frac{1}{K_F}\frac{\Gamma}{\Gamma_m - \Gamma}\exp\left(A\left(\frac{\Gamma}{\Gamma_m}\right)\right) \tag{1.5}$$

Where K_F is the Frumkin equilibrium adsorption constant, and the parameter A in a measure of the non-ideality of mixing at the interface layer. The constant A in Frumkin model is interpreted in terms of repulsive interactions between the surfactant and water molecules or attractive interactions of the hydrophobic tails of the surfactant. When A = 0, the surface is ideal, and the Frumkin isotherm reduces to the Langmuir isotherm. For $A \neq 0$, Γ_m of the Frumkin model is not the same as of the parameter Γ_m derived from Langmuir's isotherm.

Using the Gibbs adsorption equation for an ideal (dilute) solutions, the surface equation of state for the Henry isotherm can be derived using equation 1.1 and 1.2:

$$\Pi = \gamma_0 - \gamma = \mathrm{nRT}K_H\mathrm{C} = \mathrm{nRT}\Gamma \tag{1.6}$$

Π is the surface pressure and γ_0 is the surface tension of the pure water.

The analogue surface equation of state for the Langmuir isotherm is the Von Szyszkowski equation of state:

$$\Pi = \gamma_0 - \gamma = \mathrm{nRT}\Gamma_m \ln(1 + K_L C) \tag{1.7}$$

The surface equation of state for the Frumkin isotherm is Frumkin equation.

$$\Pi = \gamma_0 - \gamma = -\mathrm{nRT}\Gamma_m \ln\left(1 - \frac{\Gamma}{\Gamma_m}\right) \tag{1.8}$$

All the surface equations of state mentioned above can only apply to premicellar solutions (C < cmc) so that the Γ can be properly evaluated in the Gibbs adsorption equation.

The above equations can be used in dynamic surface tension studies in order to relate γ(t) to Γ(t) and provide the basis for dynamic adsorption models.

More complicated isotherms have been used for some surfactants. Table 1.2 lists the isotherms and the corresponding equation of states, with x = Γ/Γm

Table 1. 2. Adsorption Isotherms and Equations of state [46]

Isotherm	Henry	Langmuir	Volmer
Formula	Γ=K.C	$x = \frac{C}{C + a}$	$x = \frac{C}{C + a exp\,(\frac{x}{1 - x})}$
Parameters	K	Γ_m, a	Γ_m, a
Equation of	Π = RT Γ	Π = -$\Gamma_m RT \ln(1 - x)$	Π = -$\Gamma_m RT \ln\left(\frac{x}{1-x}\right)$

State		$= \Gamma_m RT(x + \frac{x^2}{2} + \frac{x^3}{3} + \frac{x^4}{4} + ..)$	$= \Gamma_m RT\ (x + x^2 + x^3 + \cdots)$
Isotherm	Frumkin		Van der Waals
Formula	$x = \frac{C}{C + aexp\ (Kx)}$		$x = \frac{C}{C + aexp\ \left(\frac{x}{1-x}\right) + kx}$
Parameters	Γ_m, a, K		Γ_m, a, K
Equation of State	$\Pi = -\Gamma_m RT[\ln(1-x) - \frac{K}{2}x^2] = \Gamma_m RT(x + (1+K)\frac{x^2}{2} + \frac{x^3}{3} + \cdots]$		$\Pi = -\Gamma_m RT\left[\frac{x}{1-x} + \frac{k}{2}x^2\right] = \Gamma_m RT[x + \left(1 + \frac{k}{2}\right)x^2 + \cdots]$
Isotherm	Generalized Frumkin		Phase Transition
Formula	$x = \frac{C}{C + aexp\ (kx^n)}$		Gaseous: $x_m = \frac{C}{C+a_m}$ Liquid: $x_1 = \frac{C}{C+a_1}$
Parameters	Γ_m, a, K, n		Γ_m, a_m, a_1, C_c
Equation of State	$\Pi = -\Gamma_m RT[\ln(1-x) - \frac{Kn}{n+1}x^{n+1}] = \Gamma_m RT(x + \frac{kn}{n+1}x^{n+1} + \frac{x^2}{2} + \frac{x^3}{3} + \cdots]$		Gaseous: $\Pi = -\Gamma_m RT \ln(1-x_m)$ Liquid: $\Pi = \Gamma_m RT[\ln(1-x_1) + \ln[\frac{a_m(a_1+C_c)}{a_1(a_m+C_c)}]$

1.2.2.4 Determination of equilibrium adsorption parameters

By applying a surface equation of state to γ(C) equilibrium data obtained from the Wilhelmy method or other methods of surface tension measurement one is able to find the best-fit equilibrium adsorption parameters for any isotherm [1].

Two important notes to mention here is that the surfactant should be extremely pure. Even small traces of impurity will affect the parameters obtained for the isotherms. As stated previously, the fitting should be applied to the data of γ vs. C curve before the cmc. After the cmc has been reached, the surface tension reaches a plateau and the analysis cannot be applied.[1]

Table 1.3 lists the adsorption equilibrium parameters of the Langmuir isotherm for various surfactant solutions as determined from equilibrium surface tension data.

Table 1. 3. Langmuir adsorption constants for various non-ionic surfactants obtained from γ(C) data [33]

Surfactant	Temperature (° C)	$\Gamma_m^* 10^6$ (mol m^{-2})	K_L ($m^3 mol^{-1}$)
C_6E_4	20	2.4	1.2*10
C_6E_5	20	1.9	9.4*10
C_6E_6	20	1.6	$6.7*10^2$
C_8E_8	15	3.9	4.7
	25	3.6	8.3
	35	3.1	1.9*10
	45	2.3	$1.2*10^2$
$C_{10}E_4$	20	3.4	$2.5*10^2$
$C_{10}E_6$	20	3.1	$2.8*10^2$
$C_{12}E_5$	20	7.5	$1.9*10^2$
$C_{12}E_6$	15	2.7	$4.3*10^3$
	20	4.4	$4.6*10^2$

	25	3.0	$2.8*10^3$
	35	3.2	$2.3*10^3$
$C_{16}E_6$	20	1.5	$1.6*10^6$
Triton X-100	22	2.9	$1.5*10^3$

The value of Γ_m varies little for the surfactants and it ranges from $1*10^{-6}$ to $10*10^{-6}$ mol/m^2 as it is shown in Table 1.3. In contrast K_L varies much more. The larger the value of the K_L, the more surface active the surfactant. The equilibrium adsorption constant K_L is the key parameter that shows the ability of the surfactant to reduce surface tension [1,33].

1.2.2.5 Dynamic adsorption models

When a new surface of a surfactant solution is created, the surface active molecules need time to move or diffuse through the bulk solution to the surface and for adsorption on to the surface.

For solutions of soluble surfactants, the dynamic adsorption behavior is governed by a two-step process [20]. The first step is the exchange of the surfactant molecules between the bulk solution and the subsurface. The second step is transfer of the surfactant molecules between the subsurface layer (the layer immediately at a thickness of few molecular dimensions only below the surface layer) and the surface. The first step is a mass transfer process (diffusion and sometimes convection) [33] while the second step is an adsorption process.

Models which consider diffusion as the only rate controlling step are called diffusion-controlled. If diffusion is assumed to be fast in comparison to the transfer of the molecules between the subsurface and the surface the model is considered to be kinetic or barrier-controlled. In mixed diffusion/kinetic-controlled both steps have the similar characteristic time.

The fundamental work of Ward and Tordai is the origin of all models of diffusion-controlled adsorption kinetics of surfactants at fluid interface [47,48]. They formulated the basic physical model and derived a solution in the form of an integral equation. All the following theoretical models were founded on that basic idea of a two-step process [49-63].

1.2.2.5.1 Diffusion-controlled adsorption model

In diffusion-controlled adsorption models, diffusion is the only mechanism needed in establishing adsorption equilibrium, in other words the time required for the transport of the surfactant molecule from the bulk to the subsurface is much longer than the time required for the equilibration between the surface and the subsurface. In this model the assumption is that there is no activation energy barrier for the transfer of the surfactant molecules between the subsurface and the surface.

In the Ward and Tordai model, the governing mass transfer equations and the initial and boundary conditions for the unsteady one-dimensional problem in planar interfaces are as follow:

$$\frac{\partial C(x,t)}{\partial t} = D\frac{\partial^2 C(x,t)}{\partial x^2} \quad 0 < x < \infty, t > 0 \tag{1.9}$$

I.C.: $$C(x,0) = C_b \tag{1.10}$$

$$\Gamma(0) = 0 \tag{1.11}$$

B.C.: $$C(\infty,t) = C_b \tag{1.12}$$

$$D(\frac{\partial C(x,t)}{\partial x})_{x=0} = \frac{d\Gamma(t)}{dt} \tag{1.13}$$

Where C is the surfactant concentration, Γ is the surface concentration, t is the time, D is the diffusivity in the bulk solution, x is the distance from the subsurface and C_b is the initial bulk concentration.

Similarly for spherical interface of radius r = b we can write the mass transfer equations as:

$$D\frac{1}{r^2}\frac{\partial}{\partial r}\left(r^2\frac{\partial C}{\partial r}\right) = \frac{\partial C}{\partial t} \qquad (r \geq b, t > 0) \tag{1.14}$$

I.C.: $$C(r,0) = C_b \tag{1.15}$$

$$\Gamma(0) = 0 \tag{1.16}$$

B.C. $$C(\infty,t) = C_b \tag{1.17}$$

$$D(\frac{\partial C(r,t)}{\partial r})_{r=b} = \frac{d\Gamma(t)}{dt} \tag{1.18}$$

Where r and t are the spherical radial coordinate and time, D denotes the diffusion coefficient, C(r,t) the bulk concentration, Γ(t) the surface concentration, b the drop radius, C_b the concentration far from the bubble.

Ward and Tordai [47,48] were the first who integrated the diffusion equation. They formulated the solution in terms of the unknown subsurface concentration $C_s(t) = C(x = 0,t)$.

The solution in planar interface is as follows:

$$\Gamma(t) = \sqrt{\frac{D}{\pi}}\{2C_b\sqrt{t} - \int_0^t \frac{C_s(\tau)}{\sqrt{t-\tau}}d\tau\} \tag{1.19}$$

Where t is time since the formation of the fresh surface, D is diffusivity and τ is a dummy variable with the units of time. C_b and $C_s(\tau)$ are the bulk concentration and the sub-surface concentration respectively. The integral term is the back-diffusion term and it is similar in form to the convolution integral.

Mysels [64] applied the superposition method and obtained an analogous equation to the planar Ward-Tordai equation. Their solution is applicable to the adsorption onto a convex spherical interface of radius r.

$$\Gamma(t) = \sqrt{\frac{D}{\pi}}\left\{2C_b\sqrt{t} - \int_0^t \frac{C_s(\tau)}{\sqrt{t-\tau}}d\tau\right\} + \frac{D}{r}\left\{C_b t - \int_0^t C_s(\tau)d\tau\right\} \tag{1.20}$$

The last term in the equation accounts for the curvature of the interface.

The equation for spherical interface was later derived by Maldarelli [34] by the method of Laplace transformation and the results are as follows:

$$\Gamma(t) = \frac{D}{r}\left[C_b t - \int_0^t C_s(\tau)d\tau\right] + 2(\frac{D}{\pi})^{1/2}\left[C_b\sqrt{t} - \int_0^{\sqrt{t}} C_s(t-\tau)d\sqrt{\tau}\right] \qquad (1.21)$$

The above equation along with the right adsorption isotherm can be used to find Γ(t) and then Γ(t) is substituted in Gibbs equation to find γ(t).

The γ(t) obtained by the solution of the diffusion equation would be compared to the experimental surface tension relaxation profiles to find the mechanism of the adsorption process.

1.2.2.5.2 Short time/Long time approximation

An analytical solution to the problem of diffusion-controlled adsorption to find γ(t) is only possible in the case of a Henry linear adsorption isotherm [65]. Solutions must be solved numerically for nonlinear isotherms. Miller and Kretzschmar were the first to propose a numerical technique to solve the diffusion-controlled adsorption process [66,67].

As mentioned above an analytical solution for the surface tension decay γ(t) cannot be obtained simply. Instead limiting laws can be used where γ(t) is close to either that of the pure solvent γ_0, or the equilibrium value of the solution γ_{eq},. For neutral molecules these approximations have been given by Fainerman et al. as [68]:

Short time approximation $$\gamma(t)_{t\to 0} = \gamma_0 - 2RTC_0\left(\frac{Dt}{\pi}\right)^{1/2} \quad (1.22)$$

Long time approximation $$\gamma(t)_{t\to \infty} = \gamma_{eq} + \frac{RT\Gamma^2}{2C_0}\left(\frac{\pi}{Dt}\right)^{1/2} \quad (1.23)$$

The parameters C_0, Γ, and D represents the bulk concentration, equilibrium surface concentration, and monomer diffusion coefficient of the surfactant.

As suggested by the above equations if the DST data from the surfactant solutions linearize when plotted as $t^{1/2}$ or $t^{-1/2}$ then it possibly suggests that the adsorption is diffusion-controlled. Therefore the diffusion coefficient can be calculated from the slopes using these short and long time approximations. However it is still not clear whether the adsorption is purely diffusion controlled over the entire time range [33,69].

The precise method to evaluate the adsorption mechanism is to use the whole DST profile rather than using the approximation approaches. In this approach the whole DST profile of the experimental data is compared with the predictions of appropriate models. The diffusion-controlled model is usually the starting point. The diffusion coefficient can be estimated by comparing the data with the predictions of the diffusion-controlled adsorption model. The method has the advantage over the approximation since the comparison is made for the entire DST curve. Therefore using the entire profile generates more reliable values for diffusivity coefficients than approximate approaches [33].

1.2.2.5.3 Kinetic-controlled adsorption

If the adsorption/desorption rate at the interface is slower than the diffusion rate, then the adsorption is the limiting step rather than diffusion.

In this case Γ is not at local equilibrium with C(0,t) as of when the diffusion was the limiting step. Usually the adsorption/desorption step is presented by means of a kinetic expression.

$$\frac{d\Gamma(t)}{dt} = r_1 - r_{-1} \qquad (1.24)$$

Where r_1 and r_{-1} are the forward adsorption and backward desorption rates.

If Langmuir formalism is used then the adsorption rate (first term in equation 1.24) is proportional to the concentration of surfactant just below the surface and the fraction of surface area unoccupied, while the desorption rate (second term in equation 1.24) is proportional to the fraction of the area covered by adsorbed surfactants. Therefore:

$$\frac{d\Gamma}{dt} = \beta \exp\left(-\frac{\mathrm{E}_a}{RT}\right) C_s(\Gamma_\infty - \Gamma) - \alpha \exp\left(-\frac{\mathrm{E}_d}{RT}\right)\Gamma \qquad (1.25)$$

Where α, β, E_a, E_d are the proportional factors and the energies of activation for adsorption and desorption respectively, Γ_∞ is the saturated surface concentration, T is the temperature and R is the gas constant.

1.2.2.5.4 Mixed kinetic adsorption

If the adsorption/desorption rate at the interface is comparable to the diffusion rate, then a model considering both diffusion and adsorption/desorption steps best describes the adsorption process. In the literature it is usually called a "diffusion-kinetics" or "mixed kinetic" model [33,70].

In this case the condition of local equilibrium between surface and subsurface is no longer valid. Therefore the isothermal boundary condition (equation 1.13 for diffusion into planar interface or 1.18 for diffusion into convex interface) has to be changed to account for the energy barrier in the adsorption/desorption step.

For mixed-kinetic adsorption Equation 1.25 must be simultaneously solved with Ward and Tordai equation to obtain $\Gamma(t)$.

1.2.2.6 Adsorption kinetics at air/water interface

There are many studies done on the mechanism of the adsorption of the different molecules at the air/water interface. Some examples and the concentration ranges that have been studied are summarized here. 1- Octylphenyl polyethoxylated alcohol (Triton X-100) (10^{-9}-10^{-7} mol/cm^3) [46] 2- Diazinon (10^{-9}-10^{-7} mol/cm^3) [36] 3- Heptadecafluoro-1-nonanol fluorinated surfactant (10^{-9} mol/cm^3) [42] 4- Straight chain ethoxylated alcohols (C_mE_n, m=10,12,14, n=4-8) (10^{-9}-10^{-7} mol/cm^3) [35,38,39,41,43,45,49,50,71-74] and (10^{-2}-10 mol/cm^3) [69] 4- Long chain normal alcohols (octanol, nonanol and decanol) (10^{-9}-10^{-6} mol/cm^3) [74,51,62], 1-

dodecanol (10^{-3} mol/cm^3)[37] 5- short chain alcohol (Propanol, Butanol, Pentanol, Hexanol) (10^{-5} mol/cm^3)[75] 6- Phosphene oxides (10^{-9}-10^{-7} mol/cm^3) [71,72,51,76] 7- Carboxylic acids (10^{-9}-10^{-6} mol/cm^3) [51,70]. 8- Sodium alkyl sulphates (from decyl up to hexa decyl) (10^{-6} mol/cm^3) [68] 9- Solfosuccinate surfactants (10^{-8}- 10^{-6} mol/cm^3) [77].

Some papers claimed diffusion-controlled mechanism and some mixed diffusion kinetic for the adsorption of the surfactants into air/water interface. However Miller claimed that the appearance of adsorption barrier is rather rare and is more probable for surfactant of a complex structure such as ionic surfactant. He stated that impurities may alter the adsorption kinetic behavior remarkably and may simulate adsorption or desorption barrier [51].

In all of the above studies the kinetic rate constants and the bulk diffusion coefficient are measured in two different experimental methods: 1- Adsorption onto a clean interface experiments where surfactant diffuses from the bulk solution and adsorbs onto a clean interface and the reduction in surface tension is measured or 2- re-equilibration experiments where the surface area of an equilibrium monolayer is changed (expanded/compressed) causing exchange with the sublayer and the re-equlibration in surface tension is measured. In these studies the common approach for analyzing the data is that the measured DST profile is compared with the prediction of diffusion model and the apparent diffusivity is computed. If the diffusivity value is reasonable (~10^{-10} m^2/s) one can infer that the adsorption is diffusion controlled. However, if the computed diffusivity is considerably smaller

than the typical value of the surfactant diffusivity in water (10^{-10} m^2/s) then the transport process is either modeled as kinetically controlled and comparison with the model yields the kinetic parameters or as mixed and kinetic constants and diffusion coefficient are derived from the fit.

Some researchers used the bubble pressure tensiometer to study the kinetics of adsorption of the surfactant at the air/water interface. They analyzed the results based on the asymptotic solutions of Ward and Tordai equation [68,69,71,72,77].The major problem in the use of bubble pressure method to study adsorption dynamics is the difficulty in the formulation of mass transport, as convection is important; however, Bendure [71] interpreted his maximum bubble pressure data according to a diffusion limited model which did not account for convection of surfactant in the liquid sublayer adjoining the expanding bubble interface, or for the area expansion of the surface. Joos and Rillaerts [72] developed a more complete equation which included the convective term. They compared their model results with the experimental data of the Bendure and confirmed the main conclusions of Bendure that the maximum bubble pressure technique is suitable for measuring adsorption kinetics. Another difference is that the dynamic surface tensions are obtained from different bubbles in the bubble pressure unit while in the shape analyzer DSTs are obtained from one stationary bubble.

Most of the literature on the study of the kinetics of adsorption using pendant drop tensiometer assumes that the surfactant bulk solution in which DST is measured is quiescent. Therefore they were able to assume that the transport of surfactant

molecule in the bulk solution is purely diffusive and they did not consider any convective term in the model. However Blankschtein et.al. [73] support the existence of convective currents in surfactant bulk solution when measuring DST using the pendant drop tensiometer.

The current study is the first study on the adsorption mechanism of sulfoxide surfactants onto a freshly created air-water interface in a quiescent solution. Pendant drop tensiometer and bubble pressure tensiometer are employed to measure the DST profiles of the surfactant solutions. DST profiles of five different concentrations from the bubble pressure tensiometer is analyzed in terms of asymptotic solutions to Ward and Tordai equation and an average diffusivity is obtained. DST profiles are obtained for the same five concentrations with the drop shape analyzer as well. The entire DST profiles from the drop shape analyzer are compared to the prediction of the diffusion model and an average diffusion coefficient is obtained from the entire DST profiles. Pre-micellar dilute concentration are used to eliminate any effect of the micelles on the kinetics.

1.2.3 Microemulsions

Microemulsions, a term first introduced by Schulman [78], are thermodynamically stable emulsions of two phases, usually a water phase and an oil phase, stabilized with emulsifiers [1,79,80]. In emulsions, which are not thermodynamically stable, the drops of the dispersed phase are generally large (> 0.1 μm) so that they often take on a milky appearance while in microemulsions droplets have a size range in

the order of 5−50 nm so these solutions often appear clear. Whether an oil and water can form a microemulsion is strongly dependent on surfactant type and structure.

Microemulsions can increase the recovery of the oil from the reservoir rock due to the ultra-low interfacial tensions that can be attained between the microemulsion-petroleum interfaces. Microemulsions have found many applications in other industries including food, cosmetic, agricultural industry etc.

A well-known classification of microemulsions is that of Winsor who identified four general types of phase equilibria for microemulsions [81,82]. In Type I microemulsions, the surfactant is preferentially soluble in water and oil-in-water (o/w) microemulsions form. The surfactant-rich water phase coexists with the oil phase; in the oil phase surfactant is only present as monomers at small concentrations. In Type II microemulsions the surfactant is mainly in the oil phase and water-in-oil (w/o) microemulsions form. The surfactant-rich oil phase coexists with a water phase where surfactant is only present as monomers at small concentrations. Type III microemulsions or middle phase microemulsions are a three-phase system where a surfactant-rich middle-phase coexists with both excess water and excess oil surfactant-poor phases assuming enough oil and water are present to form both excess phases. Type IV microemulsions are a single-phase isotropic micellar solution that forms upon addition of a sufficient quantity of surfactant.

Nonionic surfactants are excellent for formulating microemulsions, because of their high hydrophobicity and insensitivity to electrolytes, especially multivalent ions.

Other advantages of nonionic emulsifiers include low price and less foam. Nonionic surfactant microemulsions were first studied in the early 1970s [83,84], following the early ionic surfactant microemulsion studies by Shulman and co-workers [85-87]. Shinoda and Kunieda found that nonionic alcohol ethoxylates turn from water-soluble to oil-soluble in a microemulsion system upon raising temperature. Sottmann and Strey studied the ultralow interfacial tension (IFT) of alcohol ethoxylated surfactants/n-alkane/water systems, and correlated the structures of surfactants and oils with the IFT and phase behaviors [88]. Salager et al. [89-91] used octylphenol ethoxylates as the surfactant in microemulsion systems to correlate more physicochemical variables with microemulsion phase behaviors.

1.2.3.1 Hydrophilic-lipophilic difference (HLD) model

Salager et al. [90,92,93] first proposed the HLD concept as the thermodynamically derived correlation to describe microemulsion systems. The Hydrophilic-Lipophilic Difference (HLD) equation is a semi-empirical equation that describes the combination of conditions that lead to the phase inversion point. The HLD equation has two general forms for ionic and nonionic surfactants as shown below:

$$Ionic \qquad HLD = Cc + ln\ (S) - K(EACN) - f(A) - \alpha_T\,(\Delta T) \qquad (1.26)$$

$$Nonionic \qquad HLD = Cc + b * S - K(EACN) - f(A) + c_T(\Delta T) \qquad (1.27)$$

In Equation 1.26, Cc is the characteristic curvatures of surfactant which reflects the hydrophilic/lipophilic nature of the surfactant. The term ln (*S*) is the logarithm of the concentration of the electrolyte (in g/100 ml); this factor represents the charge

"shielding" effect of electrolyte due to the contraction of the double layer. EACN is the equivalent alkane carbon number which is analogous to the ACN (Alkane Carbon Number) and indicates the hydrophobicity of the oil phase. For primary alkanes, EACN is the number of hydrocarbon units. For oils other than primary alkanes, EACN is a characteristic number of the oil often determined by microemulsion test. K is an empirical constant depending on the type of surfactant head group. The value of *K* ranges from 0.1 to 0.2 for numerous surfactants–oil combinations, but a value of 0.17 is typically used for most surfactants [93,94]. $f(A)$ is a function that depends on the concentration of alcohol or more generally a cosurfactant (zero if none added as was the case in this study), The temperature factor, α_T , is typically 0.01K^{-1}, and ΔT is T–T_{ref}, where T is the temperature of the system and T_{ref} is the reference temperature (25°C).

For Equation 1.27 which applies to nonionic ethoxylated surfactants, the term Cc once again represents the characteristic curvature for the surfactant. The term b*S accounts for the "salting out" of the nonionic surfactant from the aqueous phase when the electrolyte concentration increases. K*EACN and c_T (ΔT) have the same meaning as with ionic surfactants, except c_T is much larger (generally 0.06 K^{-1} [93,95]). The large c_T is due to the weakening of the hydrogen bonds between the molecules of water and the oxygen in the ethylene oxide groups of EO based surfactant molecule when the temperature increases. The temperature coefficients α_T and c_T are associated with a different sign in HLD expression; the former means

that the hydrophilicity of the surfactant generally increases with temperature while the latter means the reverse.

The characteristic curvature (Cc) as a term was introduced by Acosta et al. [93], as an extension of the original surfactant parameter σ in the HLD, that quantifies the lipophilic and hydrophilic nature of the surfactant [96]. Cc describes not only the hydrophilic/ lipophilic nature of a surfactant, but the type of nanostructures the surfactant is likely to form at the reference conditions.

HLD = 0 represents the phase inversion point where bi-continuous network of oil and water channels has been formed (Type III microemulsion). At HLD = 0, the interfacial tension tends to reach ultralow values, the emulsion stability is reduced to a minimum, changes in oil and water solubilization capacity, viscosity, and detergency performance take place. Because of these characteristics, the microemulsion is said to be at its optimum state. Positive values of HLD indicate water-swollen reverse micelles dispersed in an oil continuous phase (w/o, Type II microemulsion) while negative values of HLD indicate oil-swollen micelles dispersed in a continuous aqueous phase (o/w Type I microemulsion).

1.2.3.2 Phase inversion temperature

The phase inversion temperature is the temperature at which the microemulsion inverts from oil in water (Type I) to water in oil (Type II) or in terms of Equation 1.27, HLD goes from being negative to being positive. The reason for this change for EO based surfactants is that the hydrogen bonding between water molecules and ethylene oxide groups of the surfactant becomes less important with increasing

temperature which in turn causes the surfactant to effectively become more hydrophobic in water. The PIT phenomena of the nonionic surfactant microemulsions has the same underlying cause as the cloud point phenomena of nonionic surfactant solutions [97].

In this study, ester sulfoxide surfactants based on 2-hydroxy-4-(methylthio) butyric acid are shown to have temperature-sensitive microemulsion phase behaviors. The phase behavior of the ternary system of water/oil/ester sulfoxide surfactant with a focus on forming microemulsions will be discussed. We further extend this study to a quaternary system of these microemulsions with an inorganic electrolyte as a fourth component. Both C10 (C_{10}ESO) and C12 (C_{12}ESO) surfactants studied contained one sulfoxide unit in the structure. Phase inversion temperatures (PITs) and interfacial tensions (IFTs) between water- and oil-rich phases are measured for ternary systems of water, oils and sulfoxide surfactants. HLD parameters of these surfactants are obtained by fitting the experimental data to semi-empirical HLD equation. The value of characteristic curvature and temperature sensitivity of C_{10}ESO and C_{12}ESO surfactants are obtained and compared with similar ethoxylated alcohol surfactants. By comparing the characteristic curvature of these surfactant to the similar ethoxylated alcohol surfactants it is shown that one sulfoxide ester moiety is equally hydrophilic as approximately five ethylene oxide groups. The temperature sensitivity of the ester sulfoxides is roughly a factor of four less than ethoxylated surfactants based on the temperature coefficient of the HLD equation.

1.3 Thesis scope

This thesis in divided into six parts. Chapter 1 is the literature review. Chapter 2 explains the experimental procedure and the materials used in this thesis. In chapter 3 the physico-chemical properties of the sulfoxide surfactants including their equilibrium surface tension, critical micelle concentration, effect of electrolyte on the critical micelle concentration, wetting and foaming properties and the laundry detergency performance will be discussed.

Since in practical applications both equilibrium and dynamic surface tensions of the surfactant are important, chapter 4 is devoted to the dynamic properties of the sulfoxide surfactants. Adsorption kinetics of the surfactant molecule at the air/water interface will be discussed in this chapter.

In chapter 5 the microemulsion behavior of the ester sulfoxides will be discussed. HLD parameters of the ester sulfoxides using hydrophilic-lipophilic equation will be found and compared to that of the alcohol ethoxylates. Chapter 6 sums up the conclusions and suggestions for the future work.

References

[1] Rosen, MJ. Surfactants and interfacial phenomena. 3rd ed. Hoboken: Wiley-Interscience; 2004.

[2] Anderson, DJ. (1966) Methyl-beta-hydroxydodecyl sulfoxide containing detergent compositions. U.S. Patent 3,290,254.

[3] Crawford, RJW. (1983) Alpha-sulfoxide and alpha-sulfone carboxyl compounds. U.S. Patent 4,395,363.

[4] Lyness, WI., O'Connor, DE. (1966) Reactions of alkali metal salts of sulfinyl carbanions and alkanesulfenates with epoxy compounds and novel compounds derived therefrom. U.S. Patent 3,288,859.

[5] Webb, ID. (1957) Sulfoxide containing detergent compositions. U.S. Patent 2,787,595.

[6] Hennaux, P., Laschewsky, A. Colloid Polym Sci. 279 (2001), 1149–1159.

[7] Hennaux, P., Laschewsky A. Colloid Polym Sci. 281 (2003), 807–814.

[8] Clint, JH. J Chem. Soc. Farad. Trans. I. 71 (1975), 1327–1334.

[9] Clint, JH., Walker, T. J. Chem. Soc. Farad. Trans. I. 71 (1975), 946–954.

[10] Aratono, M., Ohta, A., Minamizawa, H., Ikeda, N., Iyota, H., Takiue, T. J Colloid Interface Sci. 217 (1999), 128–136.

[11] Iyota, H., Todoroki, N., Ikeda, N., Motomura, K., Aratono, M. J Colloid Interface Sci.208 (1998), 203–210.

[12] Iyota, H., Todoroki, N., Ikeda, N., Motomura, K., Ohta, A., Aratono, M.J Colloid Interface Sci. 216 (1999):41–49.

[13] Matsuda, T., Asoh, Y., Villeneuve, M., Matsubara, H., Takiue, T., Aratono, M. Colloid Polym Sci. 282 (2004), 324–329.

[14] Villeneuve, M., Sakamoto, H., Minamizawa, H., Ikeda, N., Motomura, K., Aratono, M. J Colloid Interface Sci. 194 (1997), 301–310.

[15] Iyota, H., Krastev, R., Muller, RJ. Colloid Polym Sci. 283 (2005), 975–981.

[16] Iyota, H., Krustev, R., Muller, RJ. Colloid Polym Sci. 282 (2004), 1392–1402.

[17] Iyota, H., Shimada, K., Abe, K., Ikeda, N., Motomura, K., Aratono, M. J Colloid Interface Sci. 234 (2001), 322–327.

[18] Iyota, H., Tomimitsu, T. J Colloid Interface Sci. 257 (2003), 327–332.

[19] Iyota, H., Tomimitsu, T., Shimada, K., Ikeda, N., Motomura, K., Aratono, M. J Colloid Interface Sci. 299 (2006), 428–434.

[20] Dynamics of Adsorption at liquid interfaces: Theory, Experiment, Application (Studies in interface science), Dukhin SS., Kretzschmar, G., Miller, R.

[21] Tadros,THF., Surfactants in Agrochemicals, Surfactant Science Series 54, Marcel Dekker, New York, 1995.

[22] Otis,DR., Ingenito,EP., Kamm,RD., Johnson, M., American Physiological Society.0161-7567/94.

[23] Easto,J., Dalton, JS., Advances in Colloid and Interface science. 85 (2000) 103-144.

[24] Reiger MM., Rhein, LD., Surfactants in Cosmetics, Surfactant Science Series 68, Marcel Dekker, New York, 1997.

[25] El-Nokay, M., Cornell, D., Microemulsions and Emulsions in Foods, A.C.S. Symposium Series 448, 1991.

[26] Smith DH. Surfactant Based Mobility Control, A.C.S. Symposium Series 373, 1988.

[27] Rosen, MJ., Hua, XY., J. Colloid Interface Sci 139 (1990) 397.

[28] Schwuger,M., J.Am. Oil Chem. Soc., 59 (1982) 258.

[29] Oh,S.G., Shah,D. Langmuir, 8 (1992) 1232.

[30] Rosen, MJ., Hua, XY., Journal of Colloid and Interface Science. Vol. 139, No.2, 1990.

[31] Chang,CH., Franses,EI. Colloid and Surfaces, 69 (1992), 189-201.

[32] Chang,CH., Wang,NHL., Frances, EI. Colloid and Surfaces, 62 (1992), 321-332.

[33] Chang,CH., Franses,EI. Colloid and Surfaces A: Physiochemical and Engineering Aspects 100 (1995), 1-45.

[34] Lin, SY., McKeigue,SYK., Maldarelli,C. AIChE Journal, Vol. 36, No.12.(1990), 1785-1795.

[35] Lin, SY.,.Lee,YC., Yang,MW., Liu, HS.Langmuir, 19 (2003), 3164-3171.

[36] Lin, SY., Lin,LW., Chang,HC., Ku,Y. J Phy. Chem. 100 (1996), 16678-166684.

[37] Tsay,RY.,Tsai,HY.,Wu, TF., Lin,SY. Colloid and Surfaces A: Physiochem, Eng. Aspects 369 (2010),148-153.

[38] Tsay,RY., Lin, SY., Lin, LW., Chen,SI. Langmuir, 13 (1997), 3191-3197.

[39] Lee,YC., Liu,HS., Lin,SY. Colloids and Surfaces A: Phisiochem. Eng. Aspects 212 (2003),123-134.

[40] Lin, SY., Tsay, RY., Lin, LW. Chen,SI. Langmuir, 12 (1996), 6630-6536.

[41] Lin, SY.,.Lee,YC., Shao, MJ., Hsu,CT. Journal of Colloids and Interface Sci. 244 (2001), 372-376.

[42] Kuo, CC., Noskov, BA., Liao, YC., Lin,SY. Journal of Colloid and Interface Science 402 (2013), 131-138.

[43] Chang, HC., Hsu,CT., Lin, SY. Langmuir, 14 (1998) 2476-2484.

[44] Tsay, RY., Lin, SY., Chen, SI. Langmuir, 13 (1997), 3191-3197.

[45] Lin, SY. A study of the effects of cohesive forces on the sorption kinetics of surfactant by pendant drop digitization, Dissertation (1991).

[46] Lin, SY., McKeigue,K., Maldarelli, C. Langmuir, 7 (1991), 1055-1066.

[47] Ward, AFH., Tordai,L. The Journal of Chemical Physics, Vol. 14. No. 7(1946), 453-461.

[48] Ward, AFH., Tordai,L. Recueil, 71 (1952), 396-408.

[49] Pan, R. A study of surfactant equations of state and transport dynamics at the air/water interface, dissertation, (1996).

[50] Pan ,R., Green,J., Maldarelli,C. Journal of Colloid and Interface science, 205(1998),213-230.

[51] Miller, R., Lunkenheimer,K. Colloid & Polymer Sci. 264 (1986), 357-361.

[52] Miller, R., Ziller,M. Colloid & polymer Sci. 266 (1988), 532-538.

[53] Miller, R., Schano,KH. Colloid and Interface Sci. 264 (1986) 277-281.

[54] Miller, R., Kretzschmar,G. Advances in Colloids and Interface Science, 37 (1991) 97-121.

[55] Miller, R., Dukhin, SS., Kretzschmar,G. Colloid & polymer Sci. 263 (1985), 420-423.

[56] Fainerman, VB., Miller, R. Langmuir, 12 (1996), 6011-6014.

[57] Fainerman, VB., Miller, R, Joos, P. Colloid and Polymer Sci. 272 (1994) 731-739.

[58] Miller, R., Fainerman, VB., Leser,ME., Michel,M. Current opinion in Colloid & interface Science 9 (2004), 350-356.

[59] Miller, R., Lunkenheimer,K. Z.phys. Chemie, Leipzig 259 (1978), 5, S. 863-868.

[60] Lee, YC., Liou, YB., Miller,R., Liu,HS., Lin, SY. Langmuir 18, (2002) 2686-2692.

[61] Fainerman, VB., Colloids Surfaces 62, (1992) 333.

[62] Lin, SY., McKeigue,K., Maldarelli,C. Langmuir, 7 (1991), 1055-1066.

[63] Lin, SY., McKeigue,K., Maldarelli,C. Langmuir 10 (1994), 3442-3448.

[64] Mysels, KJ., J. Phys. Chem. 86 (1982), 4648-4651.

[65] Sutherland,KL. The kinetics of adsorption at liquid surfaces. Division of Industrial Chemistry, C.S.I.R.O, Melbourne (1952).

[66] Miller, R., Kretzschmar,G., Colloid & polymer Sci. 258 (1980), 85-87.

[67] Miller, R. Colloid & polymer Sci. 259 (1981), 375-381.

[68] Fainerman,VB., Makievski, AV., Miller,R. Colloids and Surfaces A: Physiochemical and Engineering Aspects, 87 (1994), 61-75.

[69] Eastoe, J., Dalton, J., Rogueda, PGA., Crooks, ER., Pitt,AR., Simister,EA. Journal of Colloid and Interface Sci. 188 (1997) 423-430.

[70] Borwankar, RP., Wasan, D. Chemical Engineering Science, Vol. 38, No. 10 (1983) 1637-1649.

[71] Bendure,RL. Journal of Colloid and Interface Science, Vol. 35, No.2, (1971), 238-248.

[72] P.Joos, E.Rillaerts, Journal of Colloid and interface Science, Vol. 79, No. 1, (1981), 96-100.

[73] Moorkanikkara,SN., Blankschtein,D. Langmuir, 25 (2009), 1434-1444.

[74] Dong, C., Hsu, CT., Chiu,CY., Lin. SY. Langmuir, 16 (2000) 4573-4580.

[75] Fainerman, V., Miller,R. Journal of Colloid and Interface science 178 (1996), 168-175.

[76] Miller, R., Schano, KH., Colloid and Polymer science, 264 (1986), 277-281.

[77] Gao, Y.,Yang, X. J. Surfact Deterg, 17 (2014), 1117-1123.

[78] Schulman, J.H., Stoeckenius, W.,Prince, L.M. , J Phys Chem, 63 (1959) 1677-1680.

[79] Fanun, M., Microemulsion properties and applications. surrfactant science series. Vol. 144.

[80] Stubenrauch, C., Microemulsions : background, new concepts, applications, perspectives. 2009, U.K. Ames, Iowa: Wiley Chichester, West Susses.

[81] Winsor, PA. Transactions of the Faraday Society 44 (1948), 376-398.

[82] Winsor, P.A. Solvent properties of amphiphilic compounds. London: Butterworths Scientific Publications (1954).

[83] Kunieda, H., Shinoda, K. Bulletin of the chemical society of Japan, 55(1982), 1777-1781.

[84] Shinoda, K., Kunieda, H. Journal of Colloid and Interface science, 42 (1973), 381-387.

[85] Schulman, J.H., Riley, D.P. Journal of Colloid Science, 3 (1948), 383-405.

[86] Schulman, J.H., Friend, J.A, Journal of Colloid Science, 4 (1949), 497-509.

[87] Stoeckenius, W., Schulman, J., Prince, L. Kolloid-Zeitschrift, 169 (1960), 170-180.

[88] Sottmann, T., Strey,R. J Chem Phys, 106 (1997), 8606-8615.

[89] Marquez, N., Graciaa, A., Lachaise, J., Salager, J.L. Langmuir, 18 (2002) 6021-6024.

[90] Salager, J.L., Marquez, N., Graciaa, A, Lachaise, J. Langmuir, 16 (2000), 5534-5539.

[91] Salager, J.L., Anton, R.E., Forgiarini, A., Marquez,L., Chap. 3. In microemulsions- Background, new concepts, applications, perspectives, in Formulation of microemulsions, Ed., 2008, Blackwell Pub.: Oxford UK. p. 84-121.

[92] Salager, J.L., Morgan, J., Schechter, R., Wade, W., Vasquez, E. Soc. Pet. Enj. J, 19 (1979), 107-115.

[93] Acosta, J.E., Yuan, J.S., Bhakta, A. S. Journal of Surfactants and Detergents, 11 (2008) 145-158.

[94] Acosta, J.E. Colloid and Surfaces A: Physiochemical and Engineering Aspects, 320 (2008) 193-204.

[95] Zarate-Munez, S., Texeire de Vasconcelos, F., Myint-Myat, K., Minchom, J., Acosta, J.E., (2016). Journal of Surfactants and Detergents 19 (2016) 249-263.

[96] Bourrel, M., Salager, J.l., Schechter, R.S., Wade, W.H. J Colloid Interface Sci, 75 (1980) 451-461.

[97] Shinoda, K., Arai, H. The Journal of Physical Chemistry, 68 (1964) 3485-3490.

2. Experimental procedure

2.1 Materials

2.1.1 Ester sulfoxide surfactants

The 2-hydroxy-4-(methylthio) butyric acid derived surfactants were synthesized and purified by Novus International. The surfactants were used as received without further purification.

2.1.2 Other surfactants

Sodium dodecyl sulfate (>99%) (SDS), cetyltrimethylammonium bromide (CTAB), NPE9 were all purchased from Sigma-Aldrich. The surfactants were used as received.

2.1.3 Other materials

Sodium chloride (>99%), Sodium citrate, ethanol (HPLC grade), methanol (HPLC grade), boric acid, propylene glycol, n-octane (>99%), n-heptane (>99%), n-hexane (95%), n-nonane (>98%), n-decane (>98%), cyclohexane (99.5%), dichloromethane (DCM, HPLC grade) were purchased from Sigma-Aldrich. Methyl cyclohexane (>99%), ethyl cyclohexane (> 98%), propyl cyclohexane (>98%) were purchased from TCI.

Sodium hydroxide (>97%) was purchased from EMD. Fluorescr Tinolux CBS-X was kindly provided by BASF. The protease, mannase and amylase were kindly provided Novozymes. The PVP K30 and PVPNO Chromabond S403E were kindly provided by Ashland Inc. All the chemicals were used without further purification. Pre-soiled fabric swatches were purchased from Testfabrics Inc. The DI water used for all experiments was purified via a Barnstead NANOpure water purification system, with the output water having a resistance of 18MΩ.

2.2 Methods

2.2.1 HPLC

HPLC analyses were performed in an Agilent 1260 system equipped with a diode array detector with acetonitrile solvent and Dionex Acclaim® Organic Acid (OA 5µm, 120Å, 4 x 150mm) column.

2.2.2 Surface tension measurement

The equilibrium surface tensions of the surfactant solutions and the critical micelle concentration were measured with the Wilhelmy plate method. The equilibrium surface tensions measured by this method were validated with the extracted data from the long-time asymptotes of the DST data from the shape analyzer.

Surface tension of the surfactant solutions were determined with the Dynamic Contact Angle Analyzer (Cahn DCA-322) using the Wilhelmy plate method at

room temperature. Square glass slides manufactured by Corning with a dimensions of 22*22 mm and thickness of 0.1 mm were used as probes. The motor speed was set to 100 μm/s. The critical micelle concentrations for the surfactant solutions were determined from the break point of γ vs. log C.

In the Wilhelmy plate method the capillary force on a glass slide at the gas/liquid interface is measured. The capillary force at its maximum as the plate is pulled upward is proportional to the surface tension, the cosine of the contact angle and the wetted perimeter. The vertical force is:

$$F = \gamma P cos\theta \qquad (2.1)$$

Where P is the perimeter and θ is the receding contact angle. F is the force and is measured continuously with a sensitive micro balance.

Measurement technique was verified by measuring the surface tension of water/air. The values of the surface tension obtained from these measurements was 72 mN/m.

2.2.3 Solubility

Solubility of the surfactants in water was assessed visually at room temperature. The mixture at each concentration was examined after at least 10 min of mild shaking and ultrasonic bath agitation to see if the surfactant had completely dissolved. Solutions were observed for 2 h after mixing to ascertain the presence of supersaturation.

2.2.4 Cloud point

The cloud point of the surfactant was determined according to ASTM D2024-09. A 1.0 wt% surfactant solution was heated to 75°C, and then cooled at a 1°C/min rate to see if phase separation occurred. The solution was held at a temperature for at least 5 min, and then visually inspected. The temperature at which the coacervate phase disappeared was recorded as the cloud point.

2.2.5 Calcium tolerance

The calcium tolerance of the surfactant at CMC in a pH=7 water solution was determined by adding various concentrations of $CaCl_2$ in the solution, cooling the solution to 4°C, and then raising the temperature back to room temperature. The solution was equilibrated for at least 1 hour, and phase behavior was assessed visually.

2.2.6 Adsorption Isotherms on solids

Adsorption isotherms were performed on a hydrophilic surface (silica, specific surface area=300m^2/g via N_2 adsorption) and a hydrophobic surface (carbon nanotubes, SMW-100 [Southwest Nanotechnology], diameter=7.8 nm, length=735nm, specific surface area=252m^2/g via N_2 adsorption). 5mL water solutions of surfactants at different concentrations were made and mixed with 75mg of adsorbent at room temperature. Mixtures were maintained at room temperature for 48h to reach equilibrium, and then the supernatant were characterized with

HPLC (Aglient 1050; Phenomenex Kintex C18 column; methanol: water=80:20; flow rate 0.7mL/min; pressure: 220bar; UV detector at 210nm) to avoid any unwanted interference from contamination. The adsorption density was calculated with the equation:

$$\Gamma = Adsorption\ density = \frac{m_{sur,0} - m_{sur,super}}{A_{ads}} \tag{2.2}$$

Where $m_{sur,0}$ is the mass of surfactant in the solution before adsorption, $m_{sur,super}$ is the mass of surfactant in the supernatant after adsorption and A_{ads} is the surface area of adsorbent. Adsorption density was plotted against the equilibrium supernatant concentration. The adsorption isotherms were fitted with a two-step model described by the equations below considering both monomer adsorption and surface micellization[1]:

$$\Gamma = \frac{\Gamma_m k_1 C_e \left(\frac{1}{n} + k_2 C_e^{n-1}\right)}{1 + k_1 C_e (1 + k_2 C_e^{n-1})} \tag{2.3}$$

Where Γ_m is saturated adsorption density, k_1 is the equilibrium constant of monomer adsorption, k_2 is the equilibrium constant of surface micellization, C_e is the equilibrium surfactant constant and n is the average number of monomers in the surface micelles. The standard free energy of monomer adsorption (ΔG_m^0) and surface micellization (ΔG_{sm}^0) was calculated from the equation below:

$$\Delta G_m^0 = -RTln(k_1) \tag{2.4}$$

$$\Delta G^0_{sm} = -\left(1/n\right)RTln(k_2) \quad (2.5)$$

2.2.7 Ross-Miles foaming

The Ross-Miles foam test was run according to the test protocol given by ASTM D1173-07[2]. 50 mL of surfactant solution, also known as the receiver, was carefully poured into the 1 meter glass column, without creating any foam. A 200 mL pipette with the surfactant solution was placed 90 cm above the receiver and the solution was allowed to drop into the foam receiver. The height of the foam produced was measured immediately and after 5 min.

2.2.8 Foam collapse profile

In order to study the foam collapse profile, an apparatus similar to that in Lunkenheimer et al. was built [3]. A cylindrical glass funnel of 30 mm inner diameter and 25 cm length with a sintered glass G3 plate at the bottom was used. 50 mL of surfactant solution was slowly poured into the funnel without creating any foam. 50 mL of air was then injected with a syringe through the sintered glass plate at a 10 mL/min rate, to forcibly create 100 mL of foam. The volume of the entire air/liquid mixture (V_{total}) and that of the excess solution on the bottom (V_{excess}) was recorded. From V_{total} and V_{excess}, the volume of foam (V_f) and the foam quality (Q) can be calculated.

$$V_f = V_{total} - V_{excess} \quad (2.6)$$

$$Q = \left(1 - \frac{50mL - V_{excess}}{V_f}\right) \times 100\% \quad (2.7)$$

A model considering gravitational draining and gas diffusion by Monslave and Schechter, and Lawrence et al. [4,5] was used to fit the foam profile data:

$$V_f = V_{f,initial} \cdot (C_A e^{-K_A t} + C_B e^{-K_B t}) \quad (2.8)$$

$$C_A + C_B = 1 \quad (2.9)$$

Where 100mL is the total initial foam volume, C_A and K_A are the proportion and rate constant of foam collapse due to gas diffusion between bubbles, and C_B and K_B are the proportion and rate constant of foam collapse due to gravitational draining.

2.2.9 Draves wetting test

The Draves wetting test was run according to ASTM D2281-68 [6]. 500 mL of surfactant solution was poured into a 500 mL graduated cylinder (38 cm in height), and 5.0 g of a standard skein hooked with a lead anchor was dropped in the solution. The skein floats in the solution because of the trapped air and sinks when wetted, and the time it took to sink after initially being added to the solution was recorded as the time of wetting.

2.2.10 Laundry performance

Laundry performance was evaluated with a terg-o-tometer. The temperature was stabilized at 30°C with a water bath. The laundry detergency formulation was dosed at 3 g/l in 1 L of the tap water in terg-o-meter cylinder. The washing cycle was 20 minutes followed by a 5 minute rinsing cycle. The reflectance at 460 nm of the soiled fabrics was measured with a photoelectric colorimeter (HunterLab, UltraScan VIS) both before and after washing. The laundry efficiency was characterized by the colorimeter method rather than weight method. The improvement in the reflectance was used to determine the laundry efficiency.

2.2.11 Small Angle X-ray Scattering (SAXS)

Small-angle scattering methods using either x-rays or neutrons are the only methods available to determine the shape and size of a non-spherical micelle. In these methods, the number of scattered x-rays or neutrons as a function of scattering angle are measured. Small-angles means that angles less than 5° are generally used. Instead of scattering angle (2θ), in small-angle scattering typically q is used where $q = 4\pi\sin\theta/\lambda$; q has the advantage of being x-ray wavelength (λ) independent. A Rigaku pinhole S-MAX3000 SAXS camera was used with a microfocus sealed tube source. A nominal 2 mm quartz capillary in a specially-designed vacuum tight cell was used to hold the sample; the background was the same cell filled with water only. The size of the beam at the sample was ~ 0.4 mm. Pixel-to-angle conversion

was determined via scattering from a silver behenate sample. Fitting of data was done using the program SASFIT.

A micelle has three relevant electron densities: the electron density of the water, the electron density of the shell, and the interior of the micelle. A morphology was assumed and the scattering pattern was fit to that morphology. In the fits, the electron density of water was fixed at the appropriate value of 334 e^-/nm^3. To determine the number of molecules/micelle, the density of the micelle was assumed to be 1 g/cm^3.

2.2.12 Dynamic surface tension measurement

2.2.12.1 Pendant drop/bubble tensiometer (Drop shape analyzer)

The experimental apparatus for pendant drop tensiometry is very simple. All that is required is syringe, needle, a camera, and a light source. A basic experimental setup is shown in Figure 2.1.

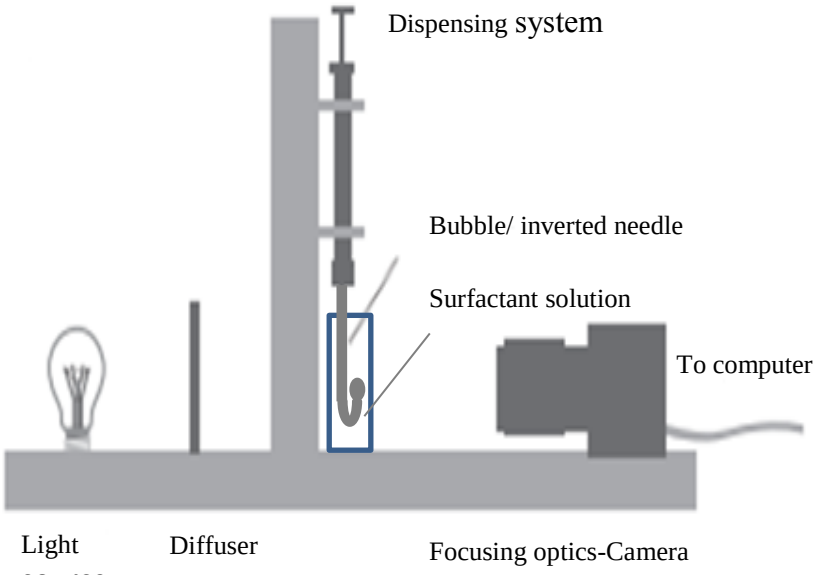

Figure 2. 1. Schematic of pendant drop tensiometer (Drop shape analyzer)

The shape analyzer experimental procedure is as follows. The quartz cell is initially filled with the aqueous solutions of the surfactant. The bubble forming inverted needle is positioned in the cell in the path of the light beam. The inverted needle immersed into the surfactant solution (4-5 ml) and a 7µl bubble was created at the tip of the needle. This setup minimizes the evaporation problem. Needle diameter was 0.72 mm. The change in the volume of the bubble is less than 5 percent as the surface tension decays over a period of 3000 s. All experiments were undertaken at 25°C. As a surfactant molecule adsorbs from the bulk solution to the freshly formed bubble surface, the surface tension of the bubble decreases as function of time. Digital images of the bubble profile are taken and the instantaneous surface tension is calculated by matching the solution of the Young-Laplace equation to the recorded bubble profile. After the surface tension relaxation was complete, the images were processed to determine the surface tension. The detailed description of pendant drop apparatus can be found in ref [7].

There is an initial dead time for the drop/bubble to form due to the dispenser system. The shape analyzer instrument time window starts from 1s theoretically but in practice with the current dispenser system it takes about 5 seconds for the instrument to create the bubble. So the instrument is not able to catch some dynamics below 5s and we lose some parts of the dynamic surface tension profile.

Although the experimental setup is simple, a number of factors must be considered to ensure that the image is of sufficient quality for precise determination of the surface/interfacial tension. To ensure that no optical aberration occurs at the drop

periphery, the light source must be diffuse. Besides reflections from the drop interface arising from overhead lighting must be avoided. For solving this problem overhead shades were used. The drop image as acquired at the digital camera sensor must be undistorted by lensing effects. The background image should be homogeneous. A typical image that is well suited to fitting is shown in Figure 2.2.

Figure 2. 2. Drop image [8]

The requirement of droplet axisymmetry is crucial for obtaining precise measurements of surface/interfacial tension. Therefore the needle must be absolutely vertical (parallel to the gravity). In particular the drop size needs to be of adequate size.

Another concern is the problem of droplet oscillation induced by both vibration and also air currents. The effect of the former was minimized with an anti-vibration table. The latter is avoided by performing the measurement in the sealed cuvette. In addition the apparatus was enclosed in a large plastic casing to avoid the air currents.

Interfacial measurement of liquid-liquid systems are much easier than the air/water interface because the inertial damping effect of a liquid continuous phase is such that vibrations are significantly less problematic.

One unavoidable feature of pendant drop tensiometry is evaporation or dissolving of one phase into another. For liquid–liquid interfacial tensions where liquid pairs of low mutual solubility are dealt with, this problem can be neglected. However, for droplets of comparatively volatile solvent in air (including water drops), evaporation is important [8].

Evaporation can be reduced by having the air saturated by moisture or perhaps using a bubble in water using the inverted needle [8]. Perhaps with evaporation compensation, the effects of evaporation could be eliminated.

To see the effect of the evaporation, Figure 2.3 shows two long time DST measurements for the CTAB. In one experiment the drop is exposed to the surrounding atmosphere while in the other the drop is sealed in a cuvette containing the experimental solution at the bottom. The purpose of this set up was to create a humid atmosphere around the drop to minimize the evaporation. Clearly, evaporation from the drop in the unsealed case causes an increase in surfactant concentration in the remaining solution, driving more surfactant to the interface and lowering the surface tension.

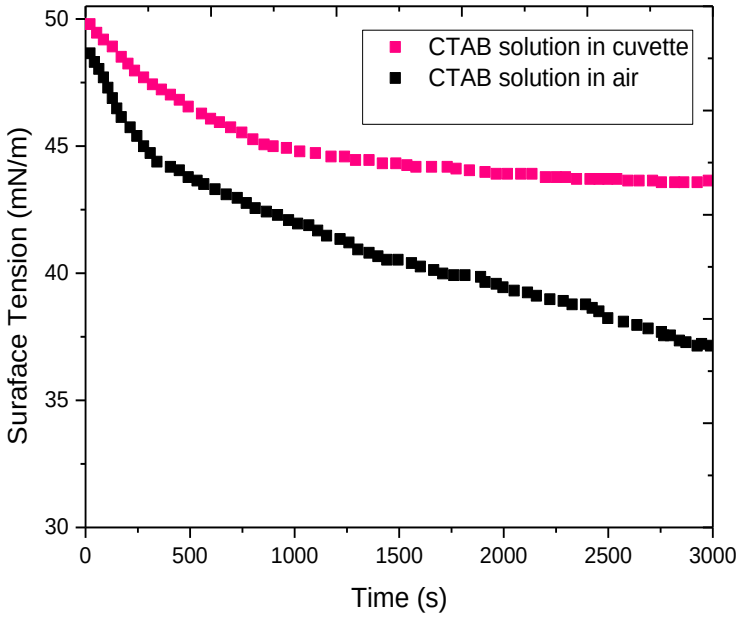

Figure 2. 3. The DST of the 0.4 mM CTAB solutions is air and in sealed cuvette at 25°C

Another important consideration is impurities. Any small traces of the impurities would result in the wrong results. For this purpose the cuvette, the tubing and the needles should be meticulously clean.

The advantage of the shape analyzer over the bubble pressure tensiometer is the small amount of the surfactant solution that is needed for the shape analyzer (3-4 ml) in contrast to 69 ml of the surfactant solution that is required for bubble pressure tensiometer experiments.

The DST measurements of surfactant solutions were done by pendant drop tensiometer (Theta OneAttension instrument) in 5s-3000s time range. The calculation are carried out automatically by OneAttension Biolin software.

2.2.12.2 Bubble pressure tensiometer

In the bubble pressure method the surface tension of a surface which is in the process of forming is measured. Gas bubbles are produced in the liquid under investigation using a capillary. During this process the pressure passes through a maximum whose value is recorded by the instrument. The time from the start of bubble formation to maximum pressure corresponds to the surface age. The surface tension as a function of surface age is measured by varying the speed of bubble formation. In Figure 2.4 the scheme of the bubble pressure tensiometer is shown. This instrument has two pressure sensors, the first to measure the gas flow and the second for the capillary pressure.

For most of the instruments the protocol consists of measuring the bubble pressure for different bubble formation frequencies. The maximum pressure P_{max} is determined from the measured signal, from which the surface tension γ at the given bubble formation time can be calculated [9]:

$$\gamma = \frac{(P_{max} - P_0)\,.\,r}{2} \qquad (2.10)$$

Here γ is the surface tension in dynes/cm (mN/m), r is the inner radius of the capillary and the nominal radius of the bubble at maximum pressure (in

centimeters), (P_{max}-P_0) is the pressure across the bubble interface in dynes/cm^2. The hydrostatic pressure (P_0) caused by immersion of the capillary tip below the surface of the liquid must be subtracted from the gage pressure to obtain the pressure drop across the interface.

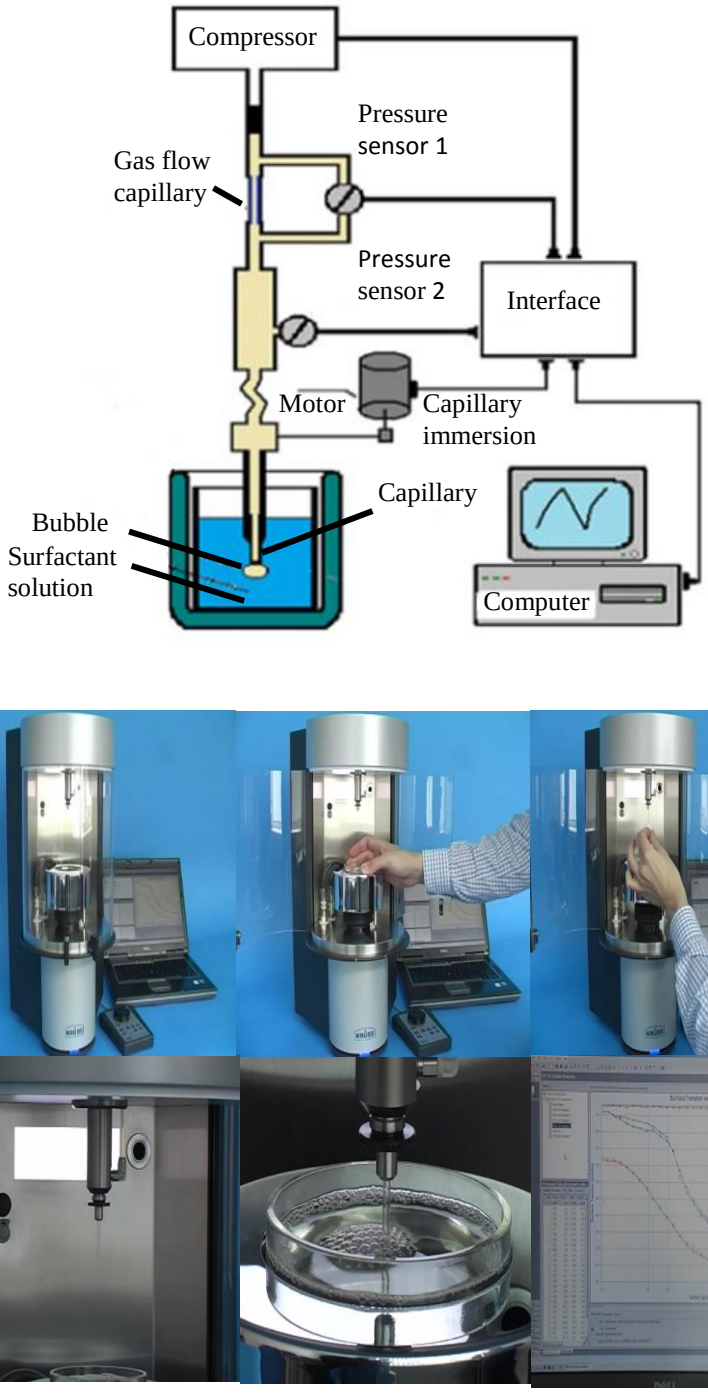

Figure 2. 4. Schematic of the bubble pressure tensiometer

The hydrostatic pressure is $\Delta\rho gh$ where $\Delta\rho$ is the density difference between the solution and air, g is the acceleration due to gravity, and h is the immersion depth. For pure water, the surface tension is independent of the bubble time and hence water provides an excellent check of the equipment.

The DST measurements of surfactant solutions are done by bubble pressure tensiometer- BP100. (Kruss, GmbH, Hamburg) in 10ms - 200s range. The diameter of the capillary used was 0.228 mm. The calculation are carried out automatically by LabDesk 3.2.2.

For the bubble pressure measurements solutions of the surfactant (at least 69 ml) were prepared and placed in the cell. The capillary size dimeter used was 0.228 mm. The capillary was immersed into the surfactant solution and the bubbles were formed at the tip of the capillary. The immersion depth is 10mm. The surface tension as the function of the surface age was calculated by the instrument. Detailed description of the bubble pressure apparatus can be found in ref [9].

2.2.12.2.1 Time-dependent pressure variation during bubble formation

In bubble pressure tensiometer the time-dependent pressure variation during bubble formation consists of four steps.

1. The bubble is formed. Initially the pressure is below the maximum pressure; the radius of curvature of the air bubble is larger than the radius of the capillary.

2. The pressure curve passes through a maximum. At this point the air bubble radius is the same as that of the capillary; the air bubble forms an exact hemisphere. The following relationship exists between the maximum pressure P_{max} the hydrostatic pressure in the capillary ($P_0 = \Delta\rho g h$), the inner radius r of the capillary and the surface tension γ.

$$\gamma = \frac{(P_{max} - P_0\ ) \,.\, r}{2} \tag{2.11}$$

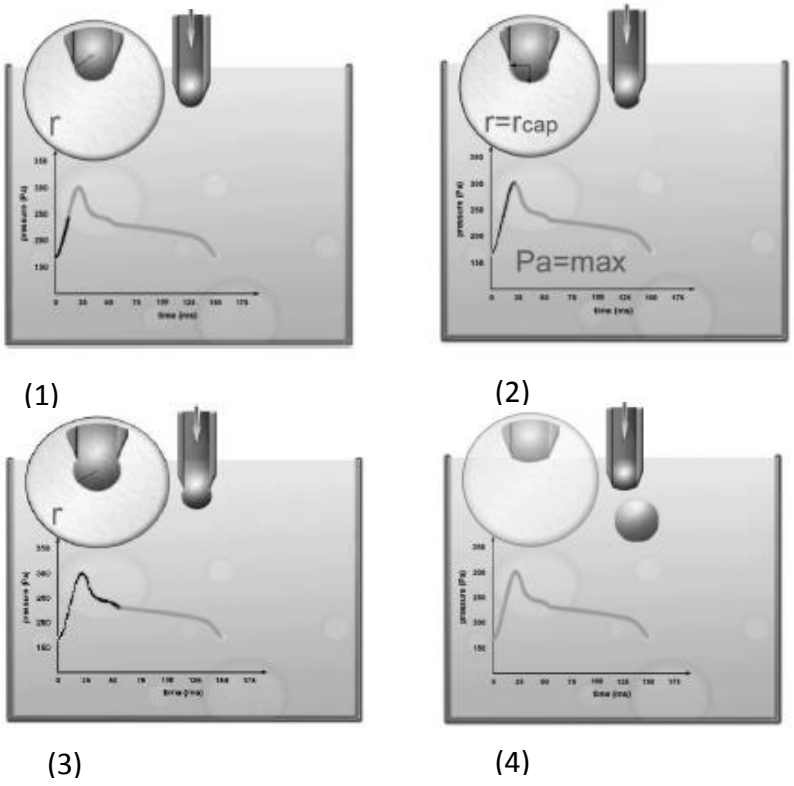

Figure 2. 5. Time-dependent pressure variation during bubble formation

3. After the maximum the “dead time” of the measurement starts. The pressure decreases again, the radius of the air bubble becomes larger.

4. The bubble finally escapes from the capillary and rises. The cycle begins again with the formation of the next bubble.

2.2.13 Interfacial tension measurement

Interfacial tension measurement (IFT) were performed with the spinning drop tensiometer M6500 Grace Instrument. Water jacket connected with thermostatic bath were used for IFT measurements at different temperatures. Relations between spinning and droplet shape in spinning drop tensiometry is illustrated in Figure 2.6. The radius of the spinning drop (R_m) at certain angular velocity (ω) is measured, and the IFT is calculated with the Vonnegut Formula [10]. The Vonnegut equation is valid if the drop is elongated with a length at least four times the diameter.

$$\gamma = \Delta\rho . \frac{\omega^2 R_m^3}{4} \qquad (2.12)$$

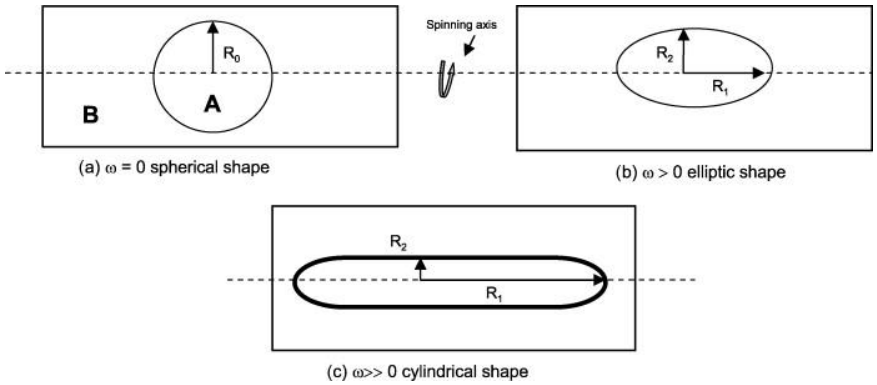

Figure 2. 6. Illustration of relations between spinning and droplet shape in spinning drop tensiometry

References

[1] Gu, T., Zhu, BY., Rupprecht, H. Surfactant adsorption and surface micellization. In: Sjoblom, J., Lindman, B., Stenius, P. (Eds.) Advances in colloid structures. Dresden: Steinkopff; (1992), 74–85.

[2] A International Standard Test Method for Foaming Properties of Surface-Active Agents-ASTM Standard Test; 2007.

[3] Lunkenheimer, K., Malysa, K., Winsel, K., Geggel, K., Siegel, S. Langmuir.26 (2009),3883–3888.

[4] Monsalve, A., Schechter, RS. J Colloid Interface Sci. 97 (1984), 327–335.

[5] Callaghan, IC., Lawrence, FT., Melton, PM. Colloid Polym Sci. 264 (1986), 423–434.

[6] A International Standard Test Method for Evaluation of Wetting Agents by the Skein Test ASTM Standard Test; 2010.

[7] Lin, SY., McKeigue, K., Maldarelli, C., AIChE Journal, Vol. 36, No.12.(1990),1785-1795.

[8] Berry, JD., Neeson, MJ., Dagastine, RR., Chan,DYC., Tabor,RF., Journal of Colloid and Interface science, 454 (2015), 226-237.

[9] Javadi,A., Mucic,N., Karbaschi,M., Won, JY., Lotfi, M., Dan, A., Ulaganathan1, V., Gochev1,G., Makievski,AV., Kovalchuk, VI., Kovalchuk,NM., Kragel,J. and Miller R., Eur. Phys. J. Special Topics 222 (2013) 7-29.

[10] Viades-Trejo, J., Gracia-Fadrique, J. Colloid and Surfaces A: Physiochemical and Engineering Aspects 302 (2007) 549-552.

3. Synthesis and characterization of novel surfactants based on 2-hydroxy-4-(methylthio) butanoic acid: non-ionic surfactants

3.1 Nomenclatures of sulfoxide compounds and their mixtures

Schematic structures of the sulfoxide esters (C_nESO) and the sulfoxide amides (C_nASO) are shown in Figure 3.1. As presented in Table 3.1, octyl 2-hydroxyl-4-(methylsulfinyl)butanoate (C_8ESO) or 2-hydroxyl-4-(methylsulfinyl)-*n*-octylbutanoamide (C_8ASO) and their analogues with longer hydrocarbon chains, namely decyl 2-hydroxyl-4-(methylsulfinyl)butanoate (C_{10}ESO), 2-hydroxyl-4-(methylsulfinyl)-*n*-decylbutanoamide (C_{10}ASO), dodecyl 2-hydroxyl-4-(methylsulfinyl)butanoate (C_{12}ESO) or 2-hydroxyl-4-(methylsulfinyl)-*n*-dodecylbutanoamide (C_{12}ASO) were mixed, because the dodecyl-/decyl-ester/amide sulfoxides are not water soluble alone at room temperature. The mixtures were named to indicate the type and fraction of the contents, as summarized in Table 3.1. For example, C_8/C_{10}ESO-70 represents a mixture of 70 wt% of C_8ESO and 30 wt% of C_{10}ESO.

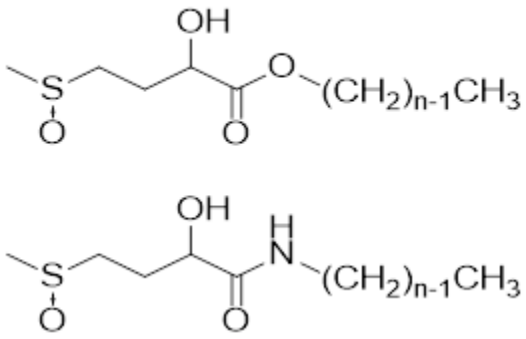

Figure 3. Molecular structure of CnESO (top) and CnASO (bottom), where n = 6, 8, 10 or 12

Table 3. 1. Contents and fraction of mixtures of sulfoxide ester/amide nonionic surfactants

Mixtures	**Contents (wt%)**	**Average Carbon Number Post Ester/Amide Groups**
C_8/C_{10}ESO-70	C_8ESO (70%) and C_{10}ESO (30%)	8.6
C_8/C_{12}ESO-70	C_8ESO (70%) and C_{12}ESO (30%)	9.1
C_8/C_{10}ASO-60	C_8ASO (60%) and C_{10}ASO (40%)	8.8
C_8/C_{12}ASO-75	C_8ASO (75%) and C_{12}ASO (25%)	8.9

3.2 Synthesis

The sulfoxide ester surfactants were prepared by Novus,by a two-step process shown in Figure 3.2 which entails an esterification reaction with a fatty alcohol followed by oxidation of the sulfide moiety to the sulfoxide. The esterification

reaction product was purified by distillation to isolate the product from the excess alcohol as well as other reaction by-products. The oxidation of the sulfide to the sulfoxide was performed using both mCPBA as well as hydrogen peroxide. The final product was purified using silica gel chromatography to obtain the purified materials.

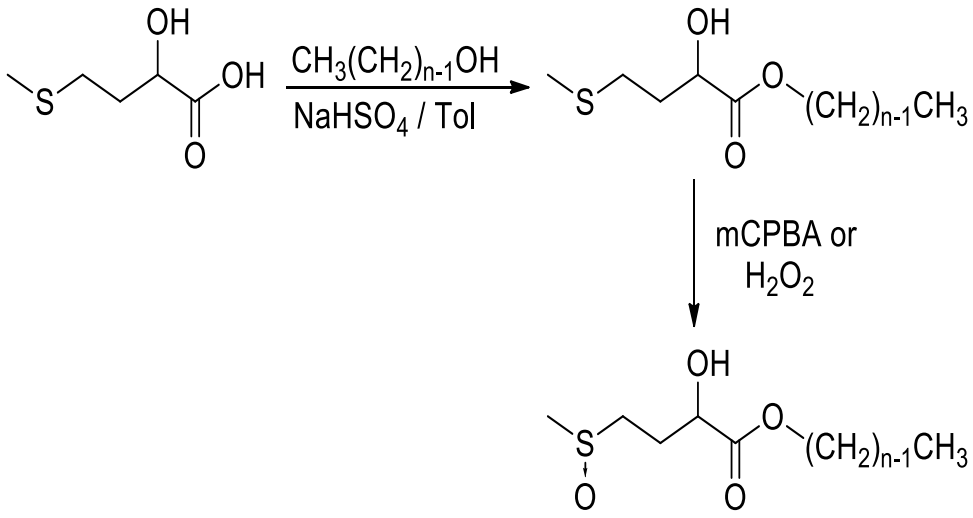

Figure 3. 1. Synthesis of CnESO and where n = 6, 8, 10 or 12

The amide synthesis is shown in Figure 3.2. In order to avoid any unwanted reactions the hydroxyl of 2-hydroxy-4-(methylthio) butanoic acid was protected through acetylation. To facilitate the coupling reaction, the carboxylic acid was then converted to the acid chloride. Reaction of the acid chloride with the appropriate amine afforded the amide. Oxidation of the sulfide to the sulfoxide was then performed with either meta-chloroperoxybenzoic acid (mCPBA) or hydrogen peroxide to give the sulfoxide in good yield. De-acytelyation of the resulting sulfoxide material using strong base gave the desired amide products. Each of the

intermediates and the final products were purified by silica gel chromatography to obtain final product with high purities. The synthesized samples were characterized with HPLC for their purity, as presented in Table 3.2. The purity of all samples was above 98% except for C_{12}ESO.

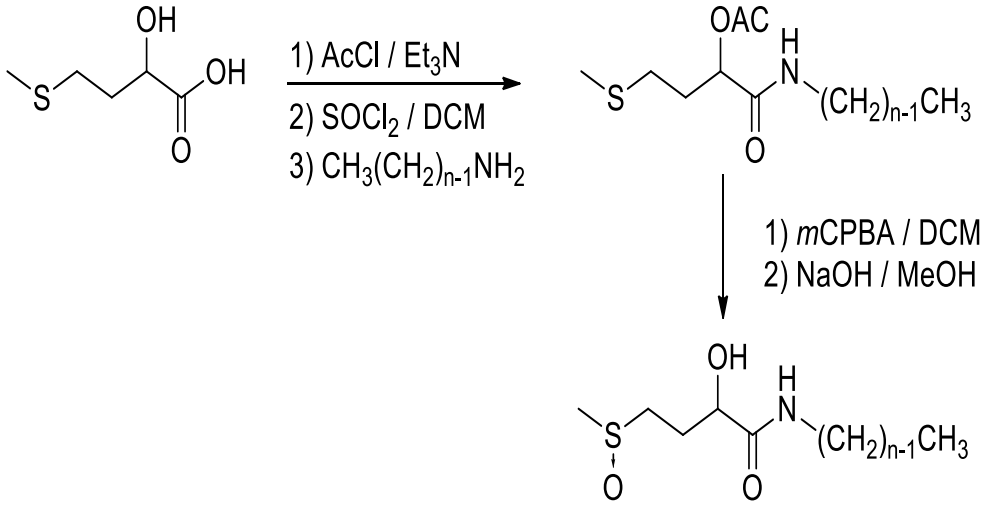

Figure 3. 2. Synthesis of CnASO, where n = 6, 8, 10 or 12

Table 3. 2. Purity of sulfoxide compounds from HPLC

Compound	**HPLC purity by area %**
C_6ESO	98.2
C_8ESO	98.9
C_{10}ESO	98.5
C_{12}ESO	94.1
C_8ASO	99.1
C_{10}ASO	99.2
C_{12}ASO	99.1

3.3 Results and discussion

3.3.1 X-ray scattering

The first step in scattering experiments was to fit sodium dodecyl sulfate to confirm that our procedures were appropriate. The fit is shown in Figure 3.3. The simplest model is a monodisperse spherical core-shell morphology; for a good fit some size polydispersity was required (the polydispersity is likely a result of smearing of the pattern due to the finite beam size). The diameter with a polydisperse spherical core-shell morphology, 2.13 nm, is within experimental error of what others have found [1]. The electron densities were reasonable for the shell, but the core was lower than appropriate, 162 e^-/nm^3 (the electron density of a typical hydrocarbon is ~300 e^-/nm^3). A fit with an ellipsoidal core-shell model had the same level of agreement, but the electron density parameters were even more unrealistic.

Fits for the C_8ESO molecule are shown in Figure 3.4 and Figure 3.5. Both the polydisperse spherical core-shell model and the ellipsoidal core-shell model gave acceptable fits to the data; however the latter had more realistic electron densities. Scattered intensities were lower for the C_8ESO vs. the SDS because the latter contains sodium in the shell. For both model fits, the size of the micelle was smaller (in the smaller dimension for the elliptical model) than SDS.

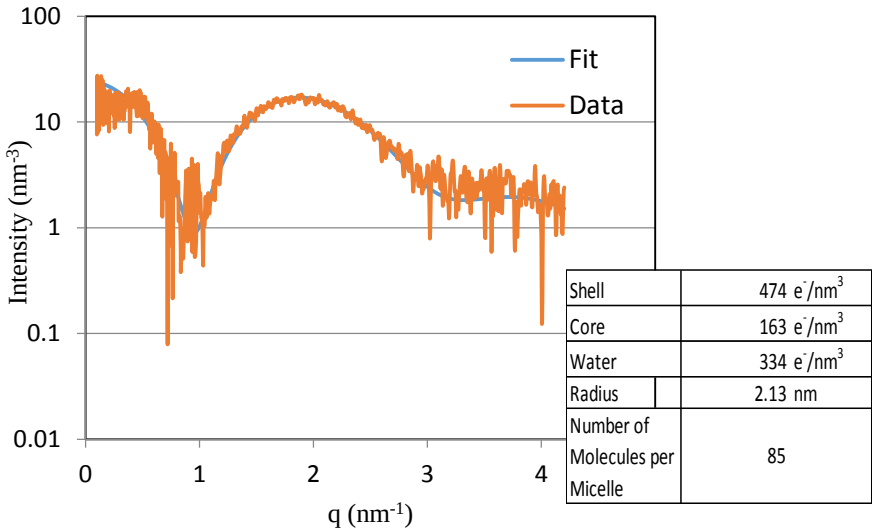

Figure 3. 3. Data and Fit for SAXS pattern from 1.25 wt. % SDS

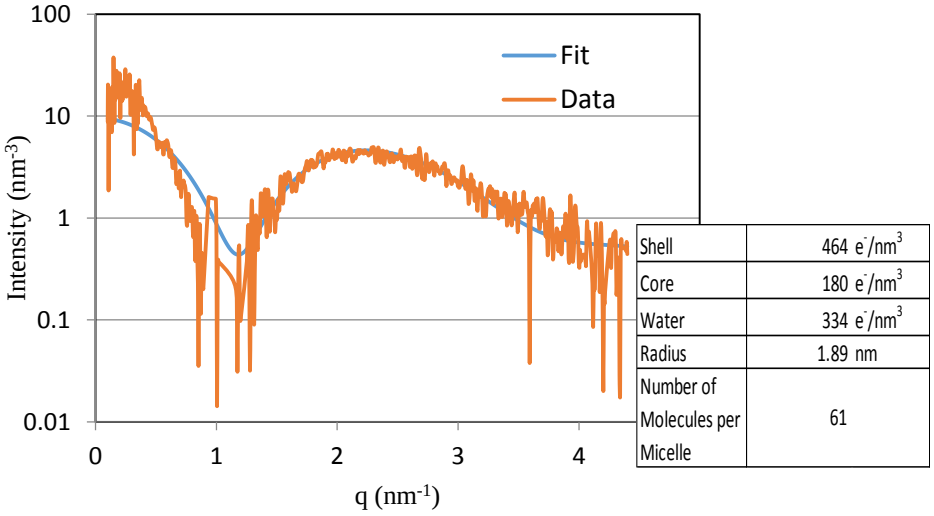

Figure 3. 4. Data and Fit for SAXS pattern from 1.3 wt.% C_8ESO

(~ 4*CMC) with polydisperse core-shell spheres

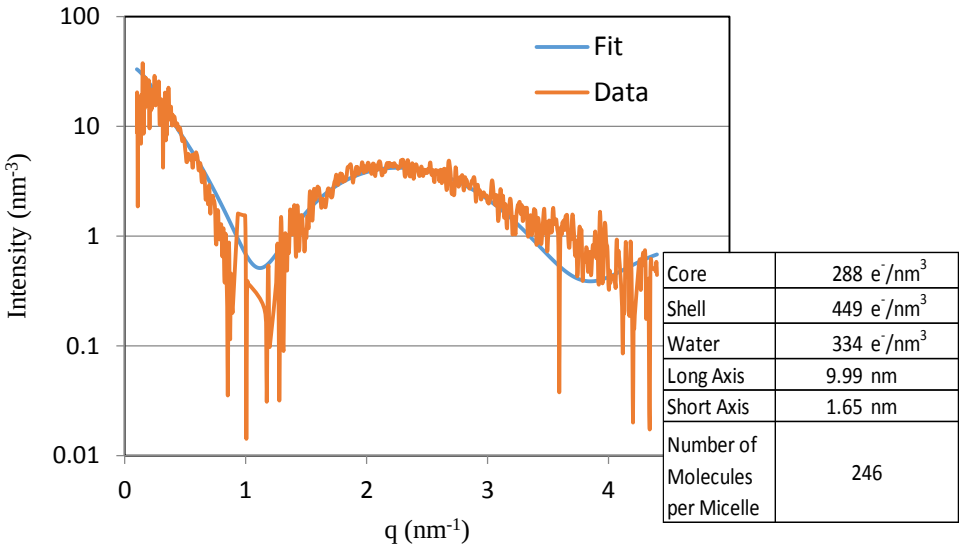

Figure 3. 5. Data and Fit for SAXS pattern from 1.3 wt.% C_8ESO

(~ 4*CMC) with ellipsoids

3.3.2 Cloud temperature

As shown in Table 3.3, sulfoxide surfactants have no observable cloud temperatures below 75°C, except those of C_8/C_{10}ESO-70 and C_8/C_{12}ESO-70, which are still higher than NPE9 and comparable to $C_{12}EO_7$. Phase separation at the cloud point is explained as a sharp increase in aggregation number [2,3] which happens when the surfactant critical packing parameter [4-6] ($V_H/l_c a_0$, where V_H is the volume in the micelle core taken by the hydrophobe, l_c is the length of the hydrophobe and a_0 is the area occupied by the hydrophilic group at the interface) approaches 1 [6]. A high cloud point of a nonionic surfactant is attributed to a small critical packing parameter and low aggregation number at room temperature [7]. The high cloud

points of these sulfoxide surfactants were a combination of three factors: straight chain hydrophobic groups, which lead to lower packing parameter; multiple hydrophilic groups in the hydrophilic groups favoring lower aggregation number and the sulfoxide's high tendency to form hydrogen bonds with water [8]. Higher cloud points of the sulfoxide based surfactants mean wider operating temperature windows and easier formulation.

Table 3. 3. Cloud temperature of sulfoxide surfactants and their mixtures

Sample	**Cloud Temperature (°C)**
C_6ESO	>75
C_8ESO	>75
C_8/C_{10}ESO-70	60
C_8/C_{12}ESO-70	57
C8ASO	>75
C_8/C_{10}ASO-60	>75
C_8/C_{12}ASO-75	>75
NPE9	53
$C_{12}EO_7$ [9]	58.5

3.3.3 Calcium tolerance

As presented in Table 3.4, both C_8ESO and C_8ASO presented extremely high tolerance against calcium ions in the solution, compared to anionic surfactants. Compatibility with multivalent ions is a signature property of nonionic surfactants, so the sulfoxide surfactants behave as nonionic surfactants at neutral pH and room temperature.

Table 3. 4. Calcium tolerance of sulfoxide compounds in comparison to various anionic surfactants

Surfactants	**$CaCl_2$ Tolerance (μM)**	**Hardness Tolerance (ppm as $CaCO_3$)**
C_8ESO	≥ 5M	≥ 5M
C_8ASO	≥ 5M	≥ 5M
C_{12}ESOCOONa[7]	5000	500
Sodium Dodecanoate [7]	0.5	0.05
SDS [10]	40 [10]	4

3.3.4 Equilibrium surface tension

Results of the surface tension vs. concentration measurements are presented in Figure 3.7 and Figure 3.8.

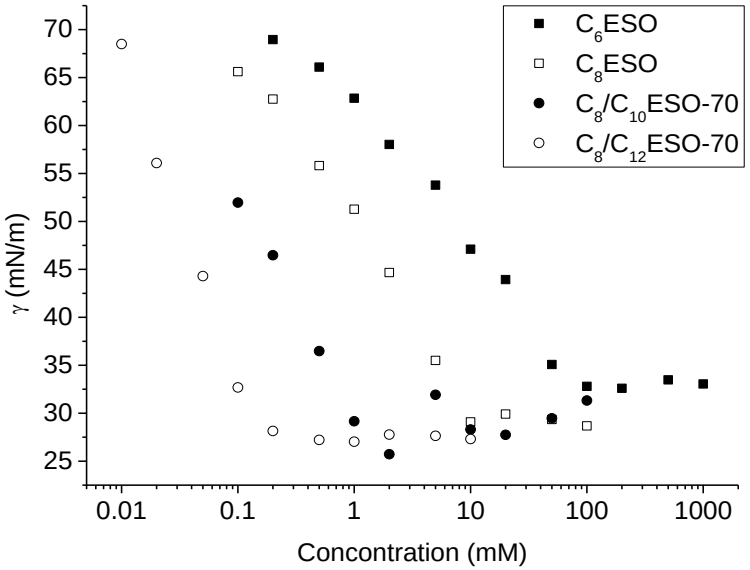

Figure 3. 6. CMC determination of C_6ESO, C_8ESO, C8/C10ESO-70 and C8/C12ESO-70 with surface tension measurement

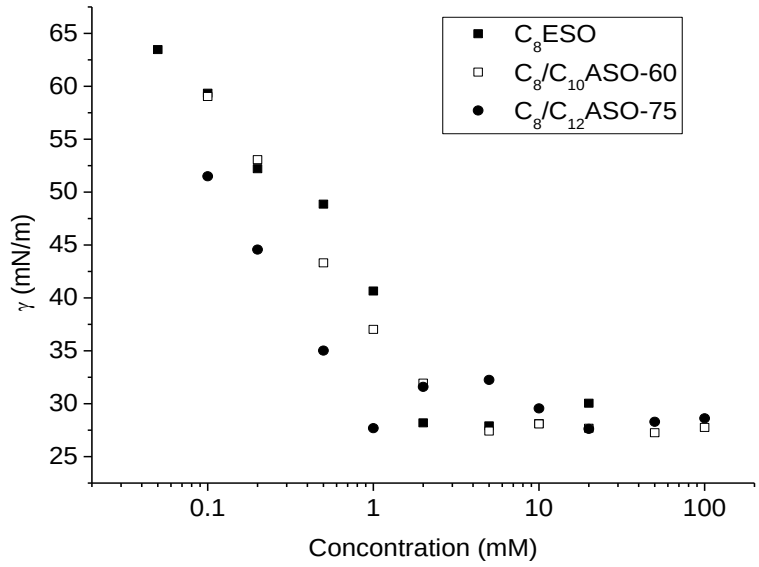

Figure 3. 7. CMC determination of C_8ASO, C8/C10ASO-60 and C8/C12ASO-75 with surface tension measurement

Surface chemical properties, including CMC, γ_{CMC}, pC20, CMC/C20, surface concentration (Γ_{max}) and minimum area per molecule at the interface (a_{min}) [7] were calculated from the γ vs. log C diagrams and are presented in Table 3.5. pC20 indicates the surface tension reduction efficiency of a surfactant, γ_{CMC} is the indicator of surface tension reduction effectiveness, and CMC/C20 indicates the tendency of a surfactant to form a micelle versus participating at the air/water interface. For calculation of Γ_m and a_{min} of the mixtures, the surfactant mixtures were treated as single component compounds. Due to solubility issues, CMCs of C_{10}ESO and C_{12}ESO were extrapolated from the CMCs of C_8ESO, C_8/C_{10}ESO-70 and C_8/C_{12}ESO-70 with the regular solution theory, assuming that mixing was ideal in the micelle phase (β^M=0). It is not clear whether C_nESO and C_nASO follow Traube's rule [11]. Sulfoxide surfactants possess relatively high pC20 indicating high efficiency in lowering surface tension. Their surface tension at the CMC and surface concentrations are comparable to other nonionic surfactants such as commercial NPE (Igepal CO-630) and hepta(oxyethylene) mono-*n*-dodecyl ether ($C_{12}EO_{7)}$, suggesting comparable effectiveness of surface adsorption. One important parameter is CMC/C20 which is an indicator of the tendency of liquid-air adsorption versus micelle formation (the higher the value, the more favored is surface adsorption). Comparison between the esters and amides indicate that the identities of these two functional groups cause no significant variation of surface chemical properties. C_8/C_{12}ESO-70 and C_8/C_{12}ASO-75 showed CMCs comparable to or lower than hepta (oxyethylene) mono-*n*-dodecyl ether ($C_{12}EO_7$, AEs) and a

commercial NPE surfactant (Igepal CO-630) with main component nona (oxyethylene) nonylphenyl ether (*NPE9*). The sulfoxide esters/amides showed lower a_{min} at the liquid-air interface than the ethoxylates.

Table 3. 5. Surface chemical properties of sulfoxide surfactants and their mixtures comparing with NPE9 and $C_{12}EO_7$

Surfactants	CMC (mM)	CMC (wt%)	γ_{CMC} (mN/m)	pC20	CMC/C20	Γ_m ($\mu mol/m^2$)	a_{min} ($Å^2$)
C_6ESO	104	2.6	33	2.4	23.9	2.5	66.9
C_8ESO	11.7 9.4[AD]	0.33	29	3.2	17.5	3.3	50.8 34.5[AD]
C_8/C_{10}ESO-70	1.1	0.037	28	4.0	12.5	4.1	41.0
C_{10}ESO	0.59*	0.018*	--	--	--	--	--
C_8/C_{12}ESO-70	0.11	0.0032	27	4.5	9.9	4.8	34.5
C_{12}ESO	0.060*	0.0020*	--	--	--	--	--
C_8ASO	6.9	0.29	29	3.3	15.4	3.5	47.3
C_8/C_{10}ASO-60	2.9	0.084	28	3.7	14.6	3.7	44.4
C_{10}ASO	1.8*	0.055*	--	--	--	--	--
C_8/C_{12}ASO-75	0.39	0.011	30	4.4	10.4	3.9	42.4
C_{12}ASO	0.16*	0.0053*	--	--	--	--	--
NPE9	0.038 0.078[AD]	0.0038	33	5.8	26.5	2.1	79.4 61.1[AD]
$C_{12}EO_7$ [9]	0.082	0.0041	34	5.3	14.9	2.9	57

Note: all data, if not referenced, were measured in our labs by surface tension measurement

AD: measured by adsorption at the solid/liquid interface

*: extrapolated from the CMCs of C_8ESO and the mixtures, assuming that β in the mixtures are all 0

3.3.5 Electrolyte effect

In aqueous solution the presence of electrolyte causes a change in CMC, the effect being more pronounced for anionic and cationic than for zwitterionic surfactants and more pronounced for zwitterionics than for nonionics. The depression of CMC for ionics is due mainly to the decrease in the thickness of the ionic atmosphere surrounding the ionic head groups in the presence of the additional electrolyte and the consequent decreased electrical repulsion between headgroups in the micelle. On the other hand the change in the CMC of nonionics and zwitterionics on the addition of electrolyte has been attributed to the salting out or salting in of the hydrophobic group in the aqueous solvent by the electrolyte [7].

Figure 3.8 shows that the CMC of C_8ESO is not a strong function of salt concentration. Poon et al.[12] reported half an order of magnitude drop in CMC for ionic surfactants with the addition of 0.2M NaCl. Therefore, the weak effect of NaCl on C_8ESO indicates that the sulfoxide does not act as an ionic surfactant in terms of aqueous micelle formation.

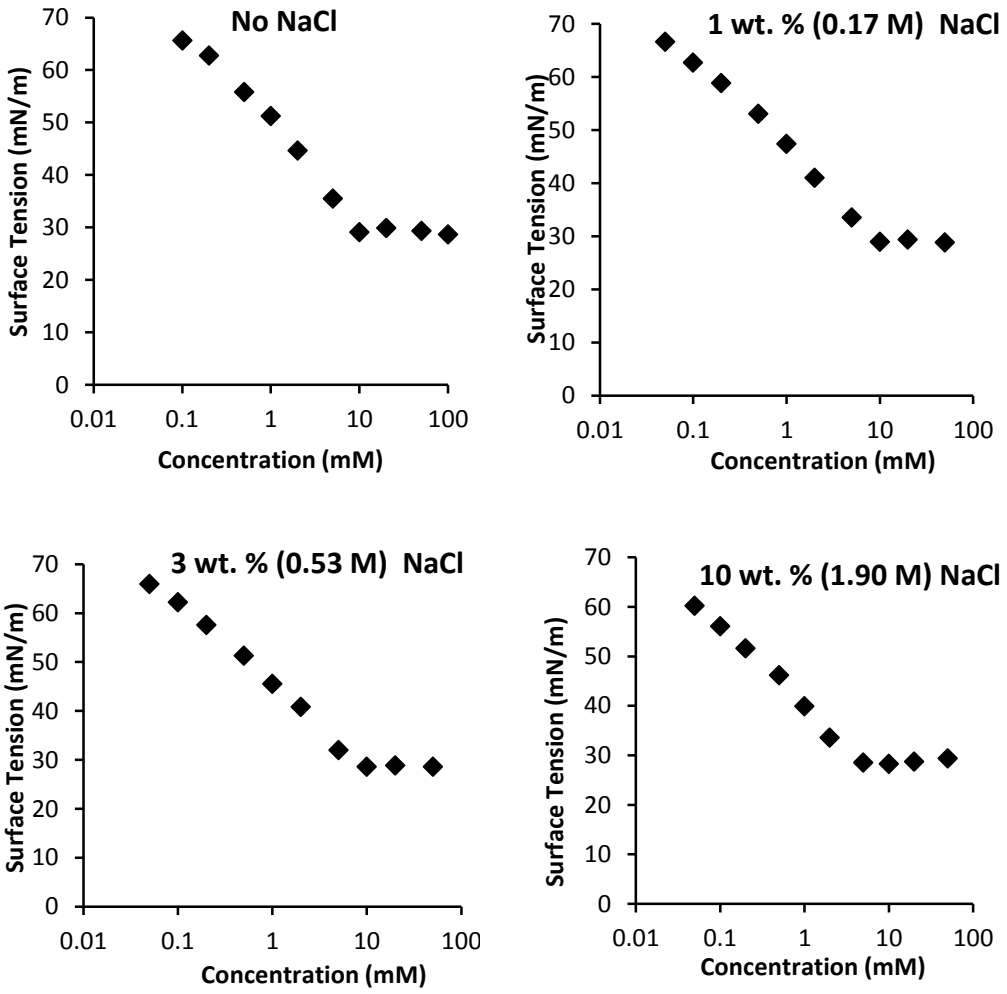

Figure 3. 8. Surface Tension vs. concentration isotherms of C_8ESO with various NaCl concentrations

3.3.6 Adsorption at the solid-liquid interface

Figure 3.10 presents adsorption isotherms of C_8ESO, NPE9 and hexa(oxyethylene) mono-*n*-dodecyl ether ($C_{12}EO_6$, AEs) onto a hydrophilic silica and hydrophobic carbon nanotubes. The a_{min} of C_8ESO and NPE9 were obtained from the curve assuming monolayer adsorption, and compared to those at the air-water interface

in Table 3.5. The a_{min} values were lower at the solid-liquid interface, which was to be expected if double layer adsorption occurred at the solid-liquid interface. However, the a_{min} values were not a factor of two lower; perhaps some of the surface area that is accessible to nitrogen adsorption is not accessible to surfactant adsorption.

Table 3. 6. Parameters in two-step adsorption model of C_8ESO and other nonionic surfactants on two solid surfaces obtained from Equation 2.3

Substrates	Surfactants	Γ_m ($\mu mol/m^2$)	k_1	k_2	n	$\Delta G_m^0/RT$	$\Delta G_{sm}^0/RT$
SMW-100	NPE9	1.71	1.76×10^4	4.02×10^{23}	6.7	-9.8	-8.1
SMW-100	$C_{12}EO_6$	2.96	1.89×10^5	2.06×10^{41}	9.2	-12.1	-10.3
SMW-100	C_8ESO	4.10	1.07×10^4	6.68×10^3	2.5	-9.3	-3.5
Aerosil-300	NPE9	2.34	1.53×10^4	1.38×10^{32}	9.5	-9.6	-7.8
Aerosil-300	$C_{12}EO_6$	4.15	4.95×10^4	1.00×10^{65}	17.4	-10.8	-8.6
Aerosil-300	C_8ESO	4.20	1.38×10^2	1.24×10^{26}	13.6	-4.4	-4.9

These adsorption isotherms were further studied by applying a two-step model [13], which takes both monomer adsorption and surface micellization into account. The model parameters of the isotherms are presented in Table 3.6. The saturated adsorption density (Γ_m) on both surfaces followed the relationship $C_8ESO>C_{12}EO_6>$*NPE9*, which is the reverse trend of a_{min} at the air/water interface. The ethoxylated surfactants have higher adsorption density on silica than carbon nanotubes. Both the standard free energy of monomer adsorption ($-\Delta G_m^0$) and

surface micellization ($-\Delta G_{sm}^0$) followed the sequence $C_{12}EO_6$>*NPE9*>C_8ESO on the surfaces.

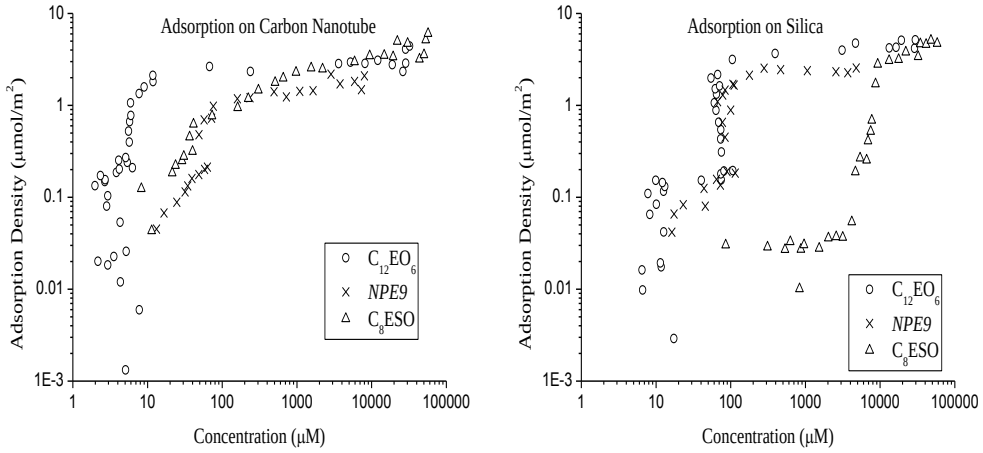

Figure 3. 9. Adsorption density of C_8ESO, NPE9 and $C_{12}EO_6$ on carbon nanotube (Left) and silica (right)

surface micellization regions followed the same trend. $-\Delta G_m^0$ positively correlates with the length of the hydrophobes of the surfactants, and is lower on the hydrophilic surface than the hydrophobic surface for the same surfactant.

3.3.7 Draves wetting performance

Table 3.7 presents the Draves wetting of the surfactant solutions. C_8ESO and C_8/C_{10}ESO-70 have comparable wetting performance at or above their CMCs as compared to NPE9. C_8/C_{12}ESO-70 wetting kinetics were slower than NPE9, and surprisingly even slower than C_8ESO. All sulfoxide surfactants had dramatically

slower wetting times when the concentration was lowered from 0.10 wt% to 0.05 wt%.

Table 3. 7. Draves wetting performance of sulfoxide ester surfactants comparing with SDS and NPE9

Wetting agent	**t_{sink} (s) @ 0.50%**	**t_{sink} (s) @ 0.25%**	**t_{sink} (s) @ 0.10%**	**t_{sink} (s) @ 0.05%**	**CMC (wt %)**
C_6ESO	>300	>300	>300	>300	2.6
C_8ESO	instant	5	>300	>300	0.33
C_8/C_{10}ESO-70	instant	6	8	>300	0.037
C_8/C_{12}ESO-70	12	21	55	>300	0.0032
SDS	instant	7	11	68	0.23
NPE9	instant	7	12	30	0.0092

3.3.8 Foaming ability and stability profile

Table 3.8 presents Ross-Miles foaming ability and foam stability of 1.0 wt% aqueous surfactant solutions. Hexyl 2-hydroxyl-4-(methylsulfinyl) butanoate (C_6ESO) presented very low foam, possibly because of its high CMC. C_8ESO created significant foam that dissipated rapidly after 5 min, while all mixtures created and maintained foam well. C_8ESO have a short hydrophobe, and form a less cohesive surface monolayer for foam stabilization.

Table 3. 8. Ross-Miles foaming property of sulfoxide surfactants and their mixtures comparing to SDS and NPE9

Sample	**Foam Height (mm)**	
	t = 0min	**t = 5min**
C_6ESO	23	2
C_8ESO	213	49
C_8/C_{10}ESO-70	206	152
C_8/C_{12}ESO-70	236	198
C_8ASO	194	99
C_8/C_{10}ASO-60	219	196
C_8/C_{12}ASO-75	213	158
SDS	206	175
NPE9	191	162

Figure 3.11 shows the foam collapse profile of 1.0 wt% surfactant water solutions.

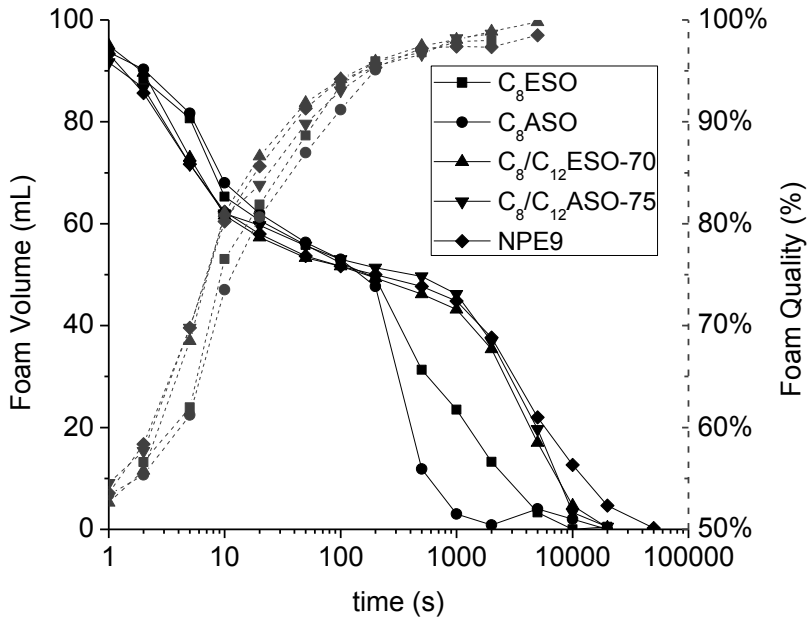

Figure 3. 10. Foam collapsing profile: foam volume (solid) and quality (dashed) generated with 1.0 wt% water solutions of C_8ESO, C_8ASO, C8/C12ESO-70, C8/C12ASO-75 and NPE9

Foam collapse profiles were fitted with the model described in the experimental section, and the parameters are presented in Table 3.9. The foams decreased in height rapidly in the first 10s due to liquid drainage, and then the decrease slowed. Beyond 10s, the foams dissipated slowly because of gas diffusion through lamellae. The start of diffusion coincided with liquid draining in lamellae effectively ceasing and Q stopping increasing. In the initial 100s, the foams of C_8ESO and C_8ASO was higher than those of C_8/C_{12}ESO-70, C_8/C_{12}ASO-75 and NPE9, and Q of the former two foams are smaller than the latter two. The observation that draining of C_8ESO and C_8ASO are slower coincides with Dreger et al.'s work that the

surfactants with faster diffusion rates creates higher initial foams in Ross-Miles foaming tests. Rosen argued quick diffusion of surfactants to the surface helps to lower the surface tension, and hence maintain the large air-water surface area in the initial foam.

Table 3. 9. Parameters of the foam collapse profile of C8ESO, C8ASO, C8/C12ESO-70 and NPE9

Surfactants	**C_A (Diffusion)**	**K_A ($\times 10^{-3}$ s^{-1}) (Diffusion)**	**C_B (Draining)**	**K_B (s^{-1}) (Draining)**
C_8ASO	0.55	4.5	0.45	0.11
C_8ESO	0.56	0.90	0.44	0.13
C_8/C_{12}ASO-75	0.56	0.22	0.44	0.20
C_8/C_{12}ESO-70	0.52	0.22	0.48	0.15
NPE9	0.53	0.18	0.47	0.18

According to the K_A values obtained in Table 3.9, gas diffusion occurred much faster in C_8ESO and C_8ASO foams than in C_8/C_{12}ESO-70 and NPE9, both the former two foams have higher C_A as well. In total, the collapse rates of the five foams goes in the order: C_8ASO > C_8ESO > C_8/C_{12}ESO-70 ≈ C_8/C_{12}ASO-75 > NPE9, which agrees with the order of K_A, the air diffusion rate, from the model fits. The permeability to air of the lamellae can be related to the arrangement of the surface monolayer and the thickness of the lamellae. C_8ASO and C_8ESO have larger a_{min} and shorter hydrophobic chains, and hence faster gas diffusion in their foams. NPE9 has a large a_{min}, but it has larger and more flexible head groups and

longer (C_{12}) hydrophobes, which can lead to a tighter and more elastic monolayer. C_8ASO foam presented a much higher diffusion rate than the other surfactants. The difference between amide and ester groups should not be the reason since C_8/C_{12}ESO-70 and C_8/C_{12}ASO-75 presented essentially the same foam collapsing profiles. The outlying behavior of C_8ASO may be due to some trace amount of foam-destabilizing impurities.

Table 3. 10. Liquid laundry formulation used in laundry test

Ingredients	**Content (wt %)**
Fatty acid	0.2
Sodium DETPMP	0.2
Sodium citrate	5
Sodium chloride	0.8
Boric acid	0.3
Propylene glycol	3
NaOH	2 (to pH=7-9)
Fluorescer	0.08
Protease	0.4
Mannase	0.15
Amylase	0.4
PVP	0.2
PVPNO	0.2
Nonionic surfactant	10
Anionic surfactant	10
Tap water	to 100%

3.3.9 Laundry performance

Laundry performance tests were done to evaluate the performance of C_8/C_{12}ESO-70 replacing NPE9 in a liquid laundry formulation. The enzyme containing liquid laundry formulation used in the current study is presented in Table 3.10. The reflectance improvement (ΔR) data of the laundry at 460nm is presented in Table 3.11. Data for the C_8/C_{12}ESO-70 containing formulation was normalized to NPE9 as shown in Figure 3.12 to compare performance between the two surfactants. Differences were apparent on some soil/fiber pairs of C_8/C_{12}ESO-70 and NPE9, but on the average, there was essentially no statistical deviation between the performances of the two surfactants. In other words, C_8/C_{12}ESO-70 was a good replacement for NPE9 based on laundry performance data in an enzyme-containing formulation.

Table 3. 11. Laundry performance (reflectance improvement at 460nm) of C8/C12ESO-70 comparing to NPE9 on cotton/polyester

Sample Soil Name	***NPE9***	***C_8/C_{12}ESO-70***
Blood/milk/ink on cotton	8.5±1.1	8.2±0.9
Tea on cotton	1.4±0.4	1.3±0.4
Coffee on cotton	2.6±0.4	3.6±0.4
Grass on cotton	18.8±1.9	19.7±2.8
Wine on cotton	14.9±0.8	15.3±0.6
Lipstick on cotton	13.5±1.7	14.1±1.8
Chocolate drink on cotton	20.5±2.3	19.6±2.2
Blood/milk/ink on PE/C	8.6±0.7	6.1±0.7
Tea on PE/C	1.7±0.6	1.4±0.4
Coffee on PE/C	3.5±0.4	3.3±0.4
Grass on PE/C	20.1±1.1	20.7±1.4
Wine on PE/C	10.8±0.6	10.2±0.5
Lipstick on PE/C	8.4±1.4	6.3±0.7
Chocolate drink on PE/C	23.2±1.8	23.5±1.5
Average	**11.2±1.0**	**11.0±1.1**

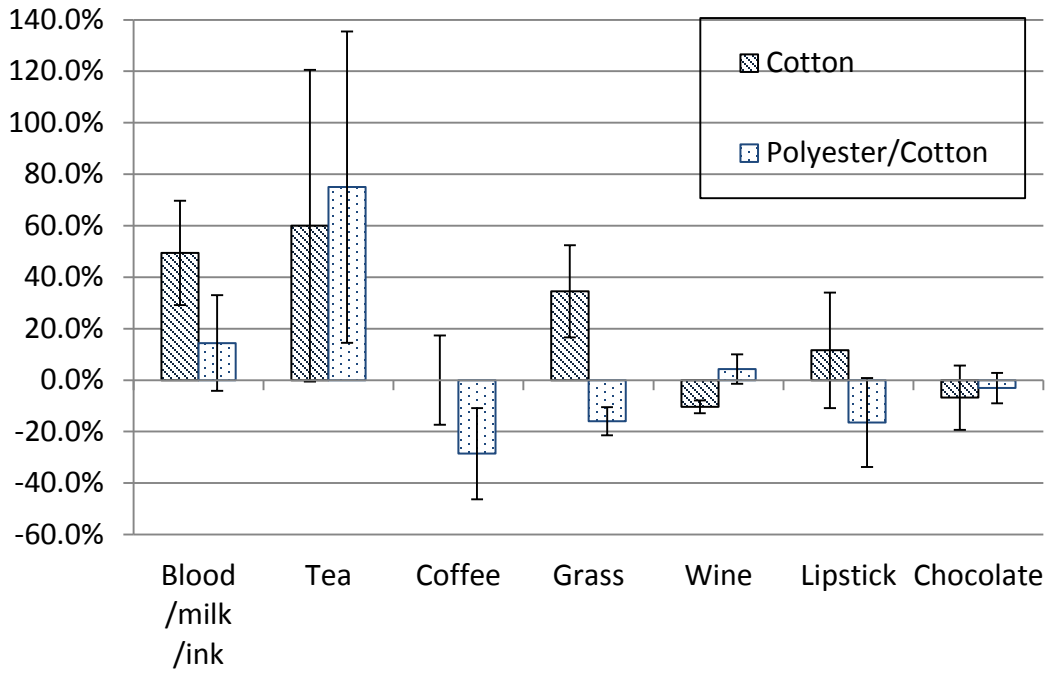

Figure 3. 11. Laundry performance (reflectance improvement at 460nm) of C8/C12ESO-70 normalized to NPE9

3.3.10 Mixtures with anionic surfactants

CMCs of binary mixtures of C_8ESO with sodium dodecyl sulfate (SDS) and with 4-(methylsulfinyl)-2-(dodecyl) butyric acid, sodium salt (C_{12}ESOCOONa) were measured. C_{12}ESOCOONa is a sulfoxide-based anionic surfactant reported by Grady *et al.* in an earlier manuscript [14]. CMCs at different mole fractions of the nonionic surfactant was analyzed according to Rubingh's one parameter model. In the model, the molecular interaction parameter (β) is used to describe the strength of the interactions. The constant β relates to the free energy change upon mixing[7]:

$$\Delta G_{mix} = \beta \mathrm{X}(1-\mathrm{X})RT \quad (3.1)$$

Where X is the mole fraction of surfactant 1 of the total surfactants in the mixture. The intermolecular interactions between two surfactants for mixed micelle or monolayer formation can be described by the following equations based on non-ideal solution theory[15]:

$$\alpha C_{12} = \mathrm{X}\mathrm{C}_1 exp[\beta(1-\mathrm{X})^2] \quad (3.2)$$

$$(1-\alpha)C_{12} = (1-\mathrm{X})\mathrm{C}_2 exp[\beta \mathrm{X}^2] \quad (3.3)$$

where α is the mole fraction of surfactant 1 in total surfactants, X is the mole fraction of surfactant 1 in the mixed micelle or the air/liquid monolayer, C_1, C_2 are the CMC or the C20 of pure surfactants 1 and 2, and C_{12} is the CMC or the C20 of the mixture. When β = 0 mixing in the micelle/monolayer is random, and when β < 0 mixing is more alternating than random. When β is negative and |β|>|log (C_1/C_2)|, there is synergism between the surfactants. The β parameter was calculated from mixed CMCs (β^M) and C20s (β^σ) with a custom-written Microsoft Visual Basic program.

Table 3.12 presents the molecular interaction parameters between C_8ESO and two anionic surfactants, sodium dodecyl sulfate (SDS) and 4-(methylsulfinyl)-2-(dodecyl) butyric acid, sodium salt (C_{12}ESOCOONa). β^M is the interaction parameter in the micelle phase and β^σ is the interaction parameter in the liquid-air monolayer. The extended application of the Rubingh's molecular interaction model [15] to the surface monolayer was proposed and done by Rosen and Hua

[16]. The more negative the β value, the more synergistic the surfactants are in this phase. Mixing of both the surfactant pairs favored micelle formation and surface tension reduction based on negative βs. Synergies were stronger, i.e. □ was more negative, for micelles vs. the surface monolayer, which is the opposite of most ethylene oxide based surfactants. This result suggests that loose micelles were formed by C_8ESO, where additional hydrophobes can be easily inserted, and in a planar formation there might be less steric effect between the tail groups. The synergy of C_8ESO with C_{12}ESOCOONa was higher than with SDS.

Table 3. 12. Molecular interaction parameters between C8ESO and two anionic surfactants

Surfactants	β^M	β^σ
C_8ESO/SDS	-1.2	-0.4
C_8ESO/C_{12}ESOCOONa	-1.9	-0.1

This chapter is collaborative work with Guangzhe Yu [17].

References

[1] Zemb, T., Charpin P. Journal De Physique, 46 (1985), 249–56.

[2] Staples, E.J., Tiddy, GT. J Chem Soc Farad Trans I., 74 (1978), 2530–2541.

[3] Tiddy, GT. Phys Rep., 57 (1980), 1–46.

[4] Israelachvili, J.N., Mitchell, D.J., Ninham, B.W. Biochim Biophys Acta., 470 (1977),185–201.

[5] Israelachvili, J.N., Mitchell, D.J., Ninham, B.W. J Chem Soc Farad Trans II. 72 (1976), 1525–1568.

[6] Mitchell, D.J., Ninham, B.W. J Chem Soc Farad Trans II. 77 (1981), 601–629.

[7] Rosen, MJ. Surfactants and interfacial phenomena. 3rd ed. Hoboken: Wiley-Interscience; 2004.

[8] Rasmussen, DH, Mackenzie, AP. Nature. 220 (1968), 1315–1317.

[9] Schott, H. J Pharm Sci. 58 (1969), 1443–1449.

[10] Stellner, KL, Scamehorn JF. Langmuir.5 (1989), 70–77.

[11] Traube, J. Justus Liebigs Annalen der Chemie. 265 (1891), 27–55.

[12] Wan, SCL, Poon PKC. Journal of pharmaceutical science, vol. 58, No.12 (1969), 1562-1567.

[13] Gu, T., Zhu, BY., Rupprecht, H. Surfactant adsorption and surface micellization. In: Sjoblom, J, Lindman, B, Stenius, P (Eds.) Advances in colloid structures. Dresden: Steinkopff; (1992), 74–85.

[14] Yu, G., Long, SA., Karinshak, KA., Grady, BP., Harwell, JH., Arhancet, GB. J Surf Deterg. 18 (2015), 895–903.

[15] Mittal, KL. Solution chemistry of surfactants. New York: Plenum; 1979.

[16] Rosen, MJ., Hua, XY. J Colloid Interface Sci. 86 (1982), 164–172.

[17] Yu,G, Shahrashoob, Z., Long, S., Liu,Y., Silva, A., Grady, B., Harwell, J., Arhancet, G.J.Surf. Deterg 20 (2017) 503-519.

4. Kinetics of adsorption of sulfoxide surfactant at air/water interface

4.1 Theoretical framework

Surfactant mass transfer along the radial direction onto a stationary spherical bubble with the appropriate boundary and initial conditions were given in chapter 1 through equation 1.14 to 1.18. Solving Equations 1.14 to 1.18 resulted in equation 1.20 for spherical interfaces [1-3].

In Equation 1.20, $C_s(\tau)$ is the instantaneous surfactant sub-surface concentration and is related to the instantaneous surfactant surface concentration Γ(t) through the equilibrium adsorption isotherm since the assumption of the diffusion-controlled model is that the sub-surface and the surface reach equilibrium instantaneously [4]:

$$\Gamma(t) = f\big(C_s(t)\big) \tag{4.1}$$

For the Langmuir isotherm we have:

$$\Gamma = \frac{\Gamma_m C_s}{C_s + a} \tag{4.2}$$

To predict Γ(t) equation 1.20 and equation 4.2 are solved simultaneously. Numerical methods are used to find Γ(t) since no analytical solution is possible for the Langmuir nonlinear isotherm. Once Γ(t) is known, the following equilibrium equation of state is used to predict the DST, γ(t).

$$\gamma_0 - \gamma_e = f\big(\Gamma(t)\big) \tag{4.3}$$

γ_0 is the pure water/air surface tension and γ_e is the equilibrium surface tension and the function $f(\Gamma(t))$ is the equation of state for the Langmuir adsorption isotherm.

4.2 Numerical solution procedure

The Ward and Tordai diffusion equation was first solved numerically by Miller and Kretschmar [5,6]. Other authors used similar approaches as that of Miller et.al. For solving the convex version of the Ward and Tordai diffusion equation numerically, Stevenson et.al. approach is opted here [7]. We first write the solution in the form of a Volterra equation [8]:

$$\Gamma(t) = g(t) + \int_0^t K(t, \tau, \Gamma(\tau))\, d\tau \tag{4.4}$$

Where
$$g(t) = C_b\left(2\sqrt{\frac{D}{\pi}t} + \frac{D}{r}t\right) \tag{4.5}$$

And

$$K\big(t, \tau, \Gamma(\tau)\big) = -\sqrt{\frac{D}{\pi}}\frac{C\big(\Gamma(\tau)\big)}{\sqrt{t-\tau}} - \frac{D}{r}C(\Gamma(\tau)) \tag{4.6}$$

Where $C(\Gamma(\tau))$ is the adsorption isotherm. For a given time increment, (h = 0.05s), if the solution at points t_i = ih , i = 0, 1, …, n-1 is known then an approximation to

$\Gamma(t_n)$ can then be computed by replacing the integral on the right hand side of Equation 4.4 by a quadrature rule using values of the integrand at t_i , i = 0, 1, …, n and solving the resulting equations for $\Gamma(t_n)$. As $\Gamma(t_0)$ = g(0), the approximate solution is computed in a stepwise manner. The numerical integration method that is used is the trapezium rule. Using the trapezium rule we need one starting value of Γ. Employing the trapezoidal rule, and discretizing equation 4.4 gives:

$$\Gamma(t_n) = g(t_n) + h(\frac{1}{2}K\left(t_n, t_0, \Gamma(t_0)\right) + \sum_{j=1}^{n-1} K\left(t_n, t_j, \Gamma\left(t_j\right)\right) + \frac{1}{2}K\left(t_n, t_n, \Gamma(t_n)\right), n = 1, 2, 3, \ldots \quad (4.7)$$

Newton-Raphson iterative method is used to solve for $\Gamma(t_n)$ within a desired accuracy range of $1*10^{-30}$. If the derivative of Γ(t) has singularities the method will not converge.

The solution is guaranteed by the fact that $\Gamma(t_{n-1})$ is always smaller than $\Gamma(t_n)$ because Γ rises monotonically and that the upper boundary is only slightly larger than $\Gamma(t_n)$.

4.3 Results and discussion

4.3.1 Determination of equilibrium adsorption parameters and surface concentration

γ vs. C are shown in Figure 4.1 for C_8ESO. The clear break in the plot defines the critical micelle concentration (cmc). If a minimum occurs near cmc in the γ vs. C

plot, it is an indicator of the presence of impurities. The equilibrium surface tensions were obtained by the Wilhelmy plate method and the values were confirmed by the long-time asymptotes of the data extracted from the shape analyzer.

The Szyszkowski surface equation of state was used to fit the $\gamma(C)$ equilibrium data obtained from the Wilhelmy plate method to obtain K_L and Γ_{max} for the Langmuir adsorption model. The pre-cmc data were used for the fit. The values for the model constants were found and listed in Table 4.1.

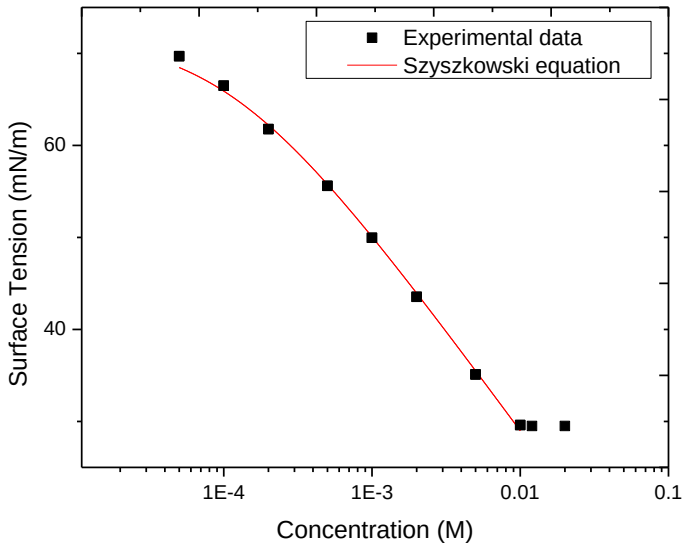

Figure 4. 1. Equilibrium surface tension vs concentration for C_8ESO

Table 4. 1. Langmuir adsorption parameters obtained from the fit to the γ(C) data.

Surfactant	$\Gamma_m^* 10^6$ (mol m^{-2})	K_L ($m^3 mol^{-1}$)
C_8ESO	3.8	8.9

The larger the value of the K_L, the more efficient or surface active the surfactant. Table 1.3 lists the values of K_L for different surfactants at different temperatures. The value of the K_L found for C_8ESO is very close to that of C_8EO_8 at 25° C. In other words, the concentration of C_8ESO required to reduce the surface tension of the solvent by 20 mN/m is the same as that of C_8EO_8.

Surface concentrations Γ(C), were obtained from the Langmuir adsorption isotherm with the calculated K_L and the Γ_{max}.

$$\Gamma(C) = \Gamma_m \frac{K_L C}{1 + K_L C} \tag{4.8}$$

Figure 4.2 shows the Γ vs C adsorption isotherm established from the above analysis.

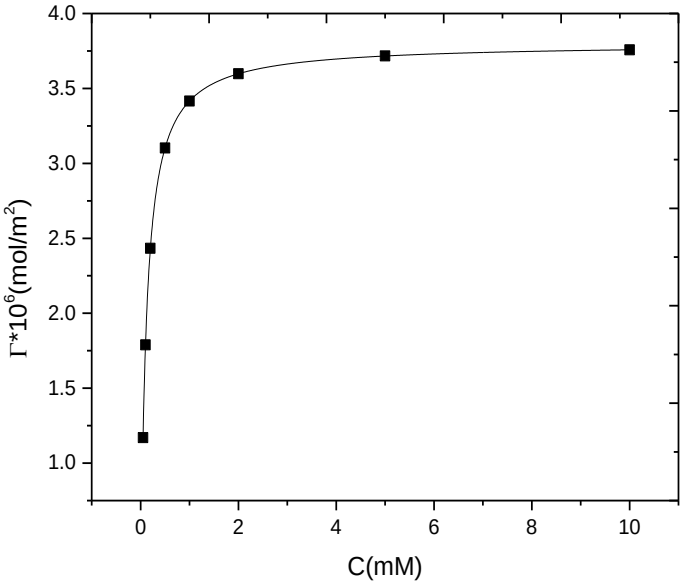

Figure 4. 2. Γ vs C for C_8ESO

4.3.2 DST from the bubble pressure tensiometer

The surface tension decay profiles of C_8ESO at the air/water interface were obtained by bubble pressure tensiometer for several concentrations of C_8ESO from 10ms up to 200s. The concentrations were chosen below the critical micelle concentration to eliminate any micelle effect. Also, the concentrations chosen need to be in a range where the concentration is high enough so that the change is not too fast so that the instrument misses the change, but also not so low that the the DST profile is too close to that of water so that no information can be determined [4].

Relaxation in the surface tension for C_8ESO at the air/water interface are plotted in Figure 4.3.

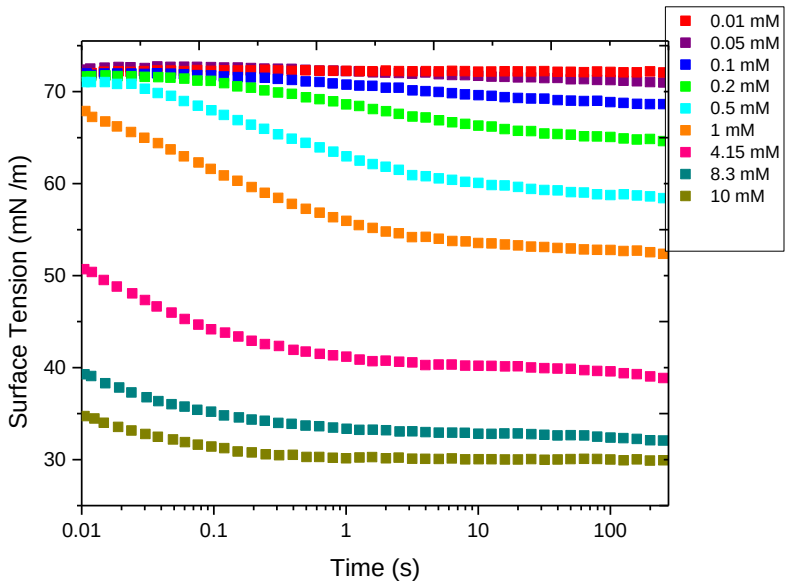

Figure 4. 3. DST data obtained by bubble pressure tensiometer for pre-cmc concentrations

As it is clear from the plot the surface tension decreases with time for all the concentrations. For high concentrations it approaches an equilibrium surface tension but for dilute solutions the surface tension decreases slowly and remain close to that of the pure solvent. As the concentration increases the DST profile becomes steeper. For higher concentrations the surface tension drops fast and the bubble pressure cannot capture the initial decay of the DST profiles from the surface tension of the pure solvent.

According to Miller et. al [9] a diffusion-controlled adsorption process would be expected to exhibit a linear plot of dynamic surface tension as a function of the reciprocal of the square root of the surface age near equilibrium, (Long time approximation). Furthermore a diffusion-controlled adsorption process would be expected to exhibit a linear plot of the dynamic surface tension as a function of the square root of the adsorption time for the initial adsorption, (Short time approximation)

Long Time Approximation: $$\gamma(t)_{t\to\infty} = \gamma_{eq} + \frac{RT\Gamma^2}{2C_0}\left(\frac{\pi}{Dt}\right)^{-1/2} \qquad (4.9)$$

Short Time Approximation: $$\gamma(t)_{t\to 0} = \gamma_0 - 2RTC_0\left(\frac{Dt}{\pi}\right)^{1/2} \qquad (4.10)$$

Therefore if the DST linearized when plotted vs $t^{1/2}$ and $t^{-1/2}$ respectively, the adsorption process is diffusion-controlled, although what happens at intermediate times cannot be conclusively stated.

The dynamic surface tension for several dilute concentrations are plotted as a function of the reciprocal of the square root of the surface age in Figure 4.4. At long times (low $t^{-1/2}$) the DST data linearize suggesting that the adsorption process is diffusion controlled. From the slope of the lines and using the equation 4.9 the diffusivities were obtained and listed in the Table 4.2.

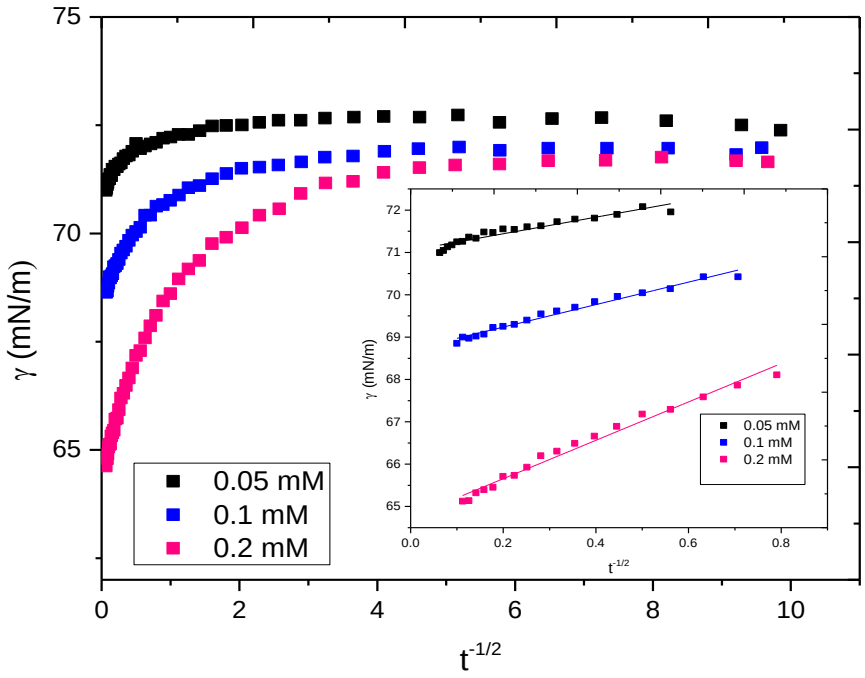

Figure 4. 4. Dynamic surface tension for C_8ESO as a function of the reciprocal of the square root of the surface age

The dynamic surface tensions corresponding to initial adsorption for the same dilute concentrations are plotted as a function of the square root of the adsorption time in Figure 4.5. The inset to the plot is the blown up of the same plot for the short time data.

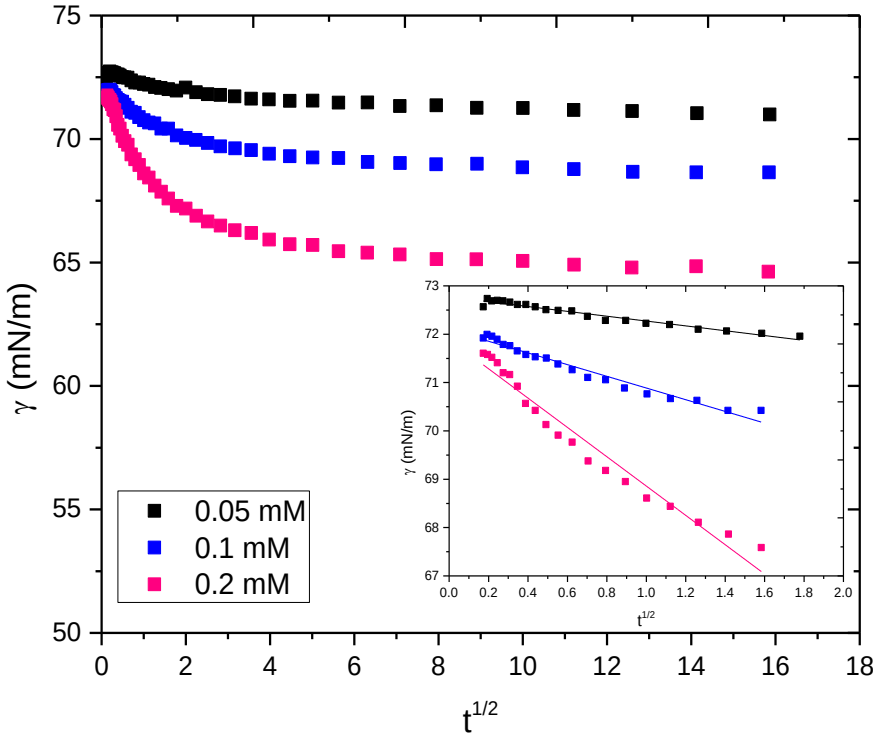

Figure 4. 5. Dynamic surface tension for C_8ESO as a function of the square root of the surface age

In the γ(t) vs $t^{1/2}$ plot, the short time data linearize as predicted by the short time approximation equation. The lines in the inset is the linear fits to the plots over an appropriate short time range. The intercept is the surface tension of the pure solvent.

From the slope of the lines and using the equation 4.10 the diffusion coefficient were obtained and listed in the Table 4.2.

Table 4. 2. Diffusion coefficients obtained from the bubble pressure DST profiles and the approximation analysis at 25°C

C_8ESO	Diffusivity coefficient $(m^2/s)*10^{-10}$	
Concentration (mM)	Long Time approximation	Short Time approximation
0.05	9.4	1.15
0.06	8.5	1.02
0.09	6.3	1.4
0.1	7	1.15
0.2	1.89	1.77

The diffusion coefficients obtained are within the range of the typical bulk phase diffusion coefficients. The typical bulk phase diffusion coefficients are $5*10^{-10}$ m^2/s. The average diffusion coefficient obtained from the short time and long-time approximation is $(3.96 \pm 3.41)*10^{-10}$ m^2/s.

The reason for the discrepancy between the short-time and long-time diffusivity data might be explained as follows. First Equation 4.9 and 4.10 which are used to find the diffusivities are just approximations and do not give the exact values for D. Second the Γ values which were substituted in Equation 4.9 to find the long-time diffusivities were not measured directly but instead fitted values were used. Third

the slope of the best fitted line to the short-time and long-time data were used to find the diffusivities which might affect the calculated values of D.

4.3.3 DST from the shape analyzer

To see whether the adsorption is diffusion-controlled over the entire time range we compared the DST data obtained by the shape analyzer over the time range of 5s-3000s with the prediction of the diffusion model. Figure 4.6 shows the DST of aqueous C_8ESO solutions for five bulk concentrations.

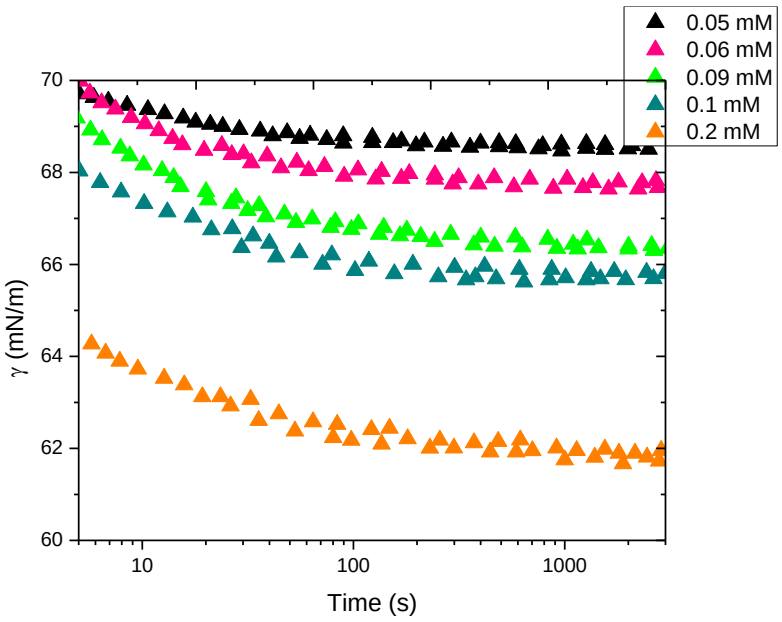

Figure 4. 6. Dynamic surface tension profiles of C_8ESO solutions obtained by shape analyzer

Numerical solution of the diffusion equation using Langmuir adsorption isotherm gives the γ(t) profiles for each concentration. Theoretical DST profiles and the

experimental DST profiles for each concentration are given in Fig 4.7-4.11 for five bulk concentrations.

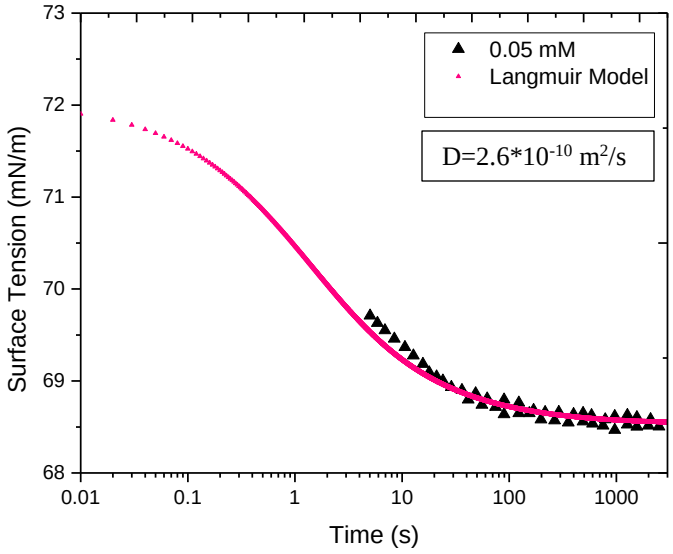

Figure 4. 7. DST profiles of 0.05 mM solution of C_8ESO using Langmuir model

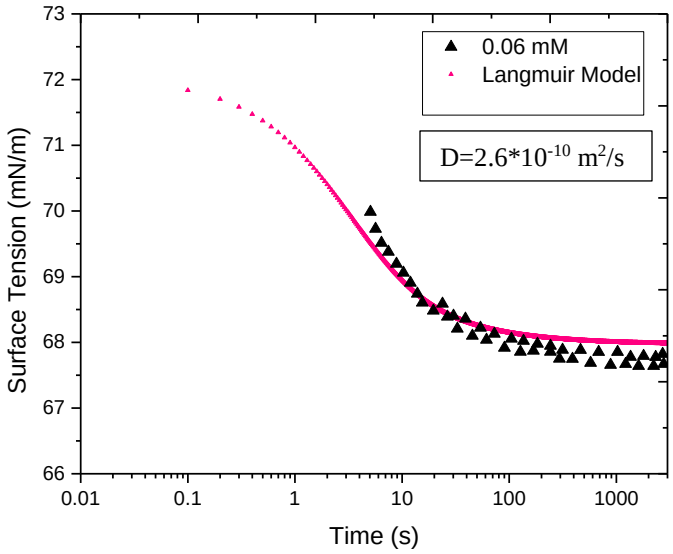

Figure 4. 8. DST profiles of 0.06 mM solution of C_8ESO using Langmuir model

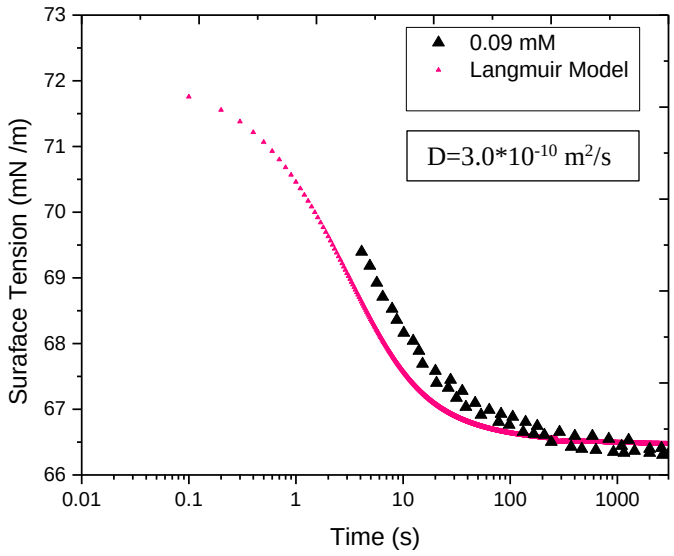

Figure 4. 9. DST profiles of 0.09 mM solution of C_8ESO using Langmuir model

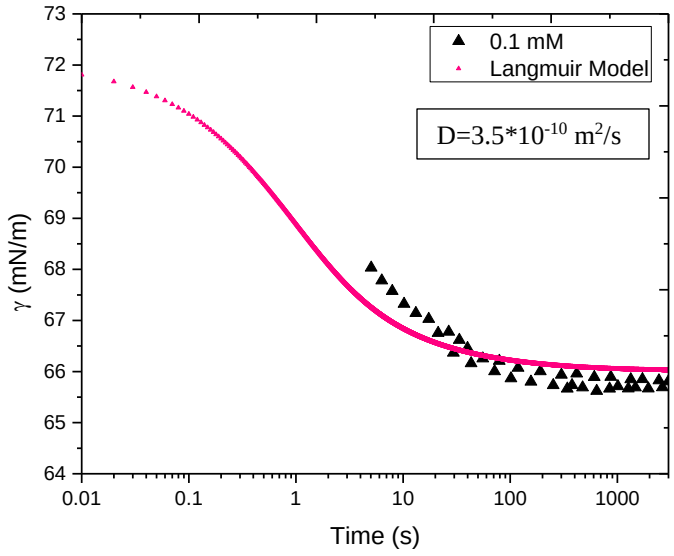

Figure 4. 10. DST profiles of 0.1 mM solution of C_8ESO using Langmuir model

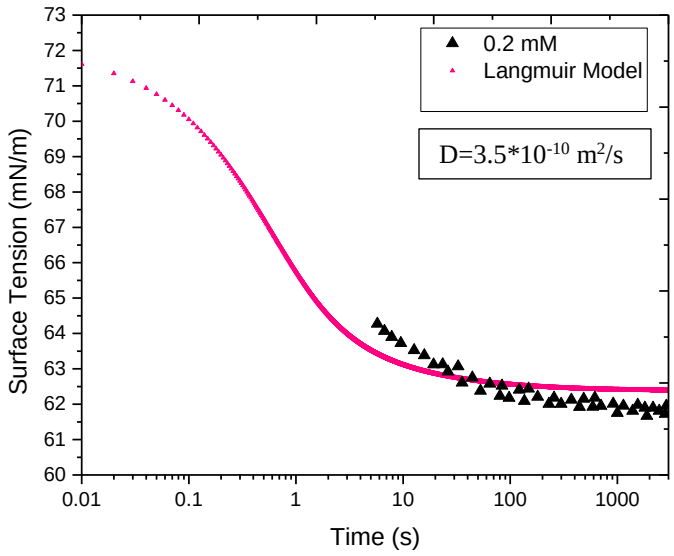

Figure 4. 11. DST profiles of 0.2 mM solution of C_8ESO using Langmuir model

The agreement achieved between the theoretical and experimental DST profiles using the Langmuir isotherm by varying the diffusion coefficient. The average diffusion coefficient of (3 ± 0.45)* 10 $^{-10}$ m^2/s gave the best fit of the theoretical to the experimental data.

The average value for the diffusion coefficient obtained from the short-time and long-time analysis of the bubble pressure tensiometer DST data was 3.96*10^{-10} m^2/s. The average diffusion coefficient obtained from fitting the theoretical profiles to the entire DST experimental data obtained by the shape analyzer is (3 ± 0.45)*10^{-10} m^2/s. Hence, the diffusion coefficient obtained from two experiments are in agreement with each other.

References

[1] Lin, SY., McKeigue, K., Maldarelli, C. AIChE Journal, Vol. 36, No.12. (1990), 1785-1795.

[2] Moorkanikkara, SN., Blankschtein, D. Langmuir, 25 (2009), 1434-1444.

[3] Lin, SY., McKeigue, K., Maldarelli, C. Langmuir, 10 (1994), 3442-3448.

[4] Dynamics of Adsorption at liquid interfaces: Theory, Experiment, Application (Studies in interface science), Dukhin, SS., Kretzschmar, G., Miller, R.

[5] Miller, R., Kretzschmar, G. Colloid & polymer Sci. 258 (1980), 85-87.

[6] Miller, R., Colloid & polymer Sci. 259 (1981), 375-381.

[7] Li, X., Shaw,R., Evans,GM., Stevenson,P. Computer and Chemical Engineering 34 (2010), 146-153.

[8] Press, WH., Teukolsky, SA., Vetterling, WT., Flannery,BP. Numerical recipes, the art of scientific computing, 3rd edition, Cambridge University Press.

[9] Fainerman, VD., Makievski, AV., Miller, R. Colloid Surface A, Physiochemical and Engineering aspects, 87 (1994), 61-75.

5. Synthesis and Characterization of Novel Surfactants Based on 2-hydroxy-4- (Methylthio) Butanoic Acid: 3. Microemulsions from Nonionic Sulfoxide Ester Surfactants

5.1 Phase inversion temperature measurement (PIT)

For microemulsion preparation, 2 wt% C_{10}ESO was solubilized in cyclohexane, methyl cyclohexane, ethyl cyclohexane, and propyl cyclohexane and mixed with DI water or DI water with added sodium chloride (1, 5, 10 wt%). For C_{12}ESO microemulsions 1 wt% surfactant was used with hexane, heptane, octane, nonane and decane. Vials at room temperature were shaken intermittently for three days to assure homogenous dispersion. The samples were then heated to 60°C and the temperature reduced to 5°C at 5°C intervals. Once an approximate PIT was identified, the same procedure was repeated except we started at a lower temperature for most samples and reduced the temperature intervals to 1°C. If a middle phase only formed at one temperature (narrow range) that temperature was used as the PIT, while if the middle phase took place at wide temperature range then the temperature corresponding to the maximum coalescence rate was assigned as the PIT. Due to safety issues (flash point of the oils) the temperature never exceeded 60°C.

5.2 Interfacial tension measurement (IFT)

The IFT is a more sensitive measure of the PIT than the method given in the previous section. At the PIT, the IFT is at its minimum value. IFT measurements were performed with a spinning drop tensiometer [1]. The radius of the spinning drop (R_m) at certain angular velocity (ω) is measured, and the IFT is calculated with the Vonnegut Formula. Vonnegut equation is valid if the drop is elongated with a length at least 4 times the diameter [2].

$$\gamma = \Delta\rho.\omega^2 R_m^3/4 \qquad (5.1)$$

5.3 Hydrophilic-lipophilic difference (HLD) parameters

Once the PITs of one surfactant vs. various oils are obtained in the absence of salt, the parameters c_T/K and Cc/K can be obtained from the linear regression of EACN vs. PIT when S = 0 and f (A) = 0 in the HLD equation:

$$EACN = C_T/K.(PIT - 25) + C_C/K \qquad (5.2)$$

Cc/K is known as the optimum EACN of an emulsifier; this ratio is equal to the EACN of the oil that forms an optimum microemulsion with the target surfactant at 25˚C with pure water. $^{C_T}/_K$ is the PIT dependence of EACN for a target surfactant. Determination of the individual K, c_T and Cc is not possible from Equation 5.2.

With HLD = 0 and with salt added four unknowns, b, Cc, c_T and K, arise from Equation 1.27. These four parameters can be obtained for ester sulfoxides using an error minimization procedure if enough (at least four) different oil/salt combinations can be found that form middle phase microemulsions with ester sulfoxides. Further details of the recursive minimization procedure used are given in the next section

5.4 Results and discussion

5.4.1 PIT

PITs of the sulfoxide surfactants/water/oil systems as well as minimum IFTs are presented in with oil/water IFT vs. temperature curves of C_{10}ESO/C_{12}ESO-alkanes presented in Figure 5.1. Type III microemulsions are formed with these systems within the temperature range of 0-60˚C. IFT of these systems are in the ultralow range ($<10^{-2}$mN/m), therefore having very high solubilization ratio according to Chun Huh relationship [3]. PITs increase with increasing EACN for both C_{10}ESO and C_{12}ESO microemulsions. Comparing to C_{12}ESO, C_{10}ESO was able to emulsify oils with lower EACN with a similar PIT (C_{12}ESO/n-octane vs. C_{10}ESO/methylcyclohexane). An increase of PIT with increasing hydrophobe length and EACN qualitatively agreed with the behaviors of EO-type nonionic surfactants in microemulsions [4-6]. Addition of sodium chloride to the aqueous phase depressed the phase inversion temperature of the emulsions for both surfactants.

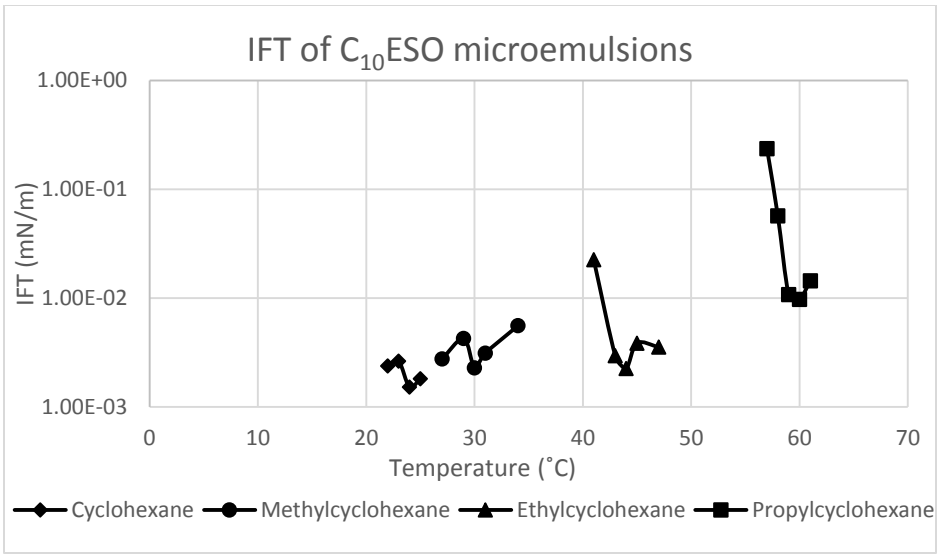

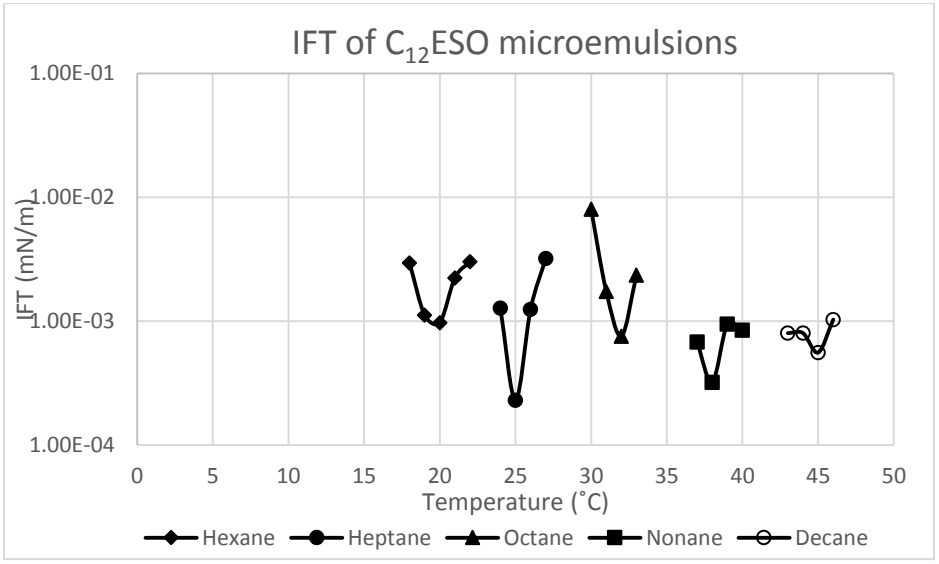

Figure 5. 1. IFT vs. temperature graphs of C_{10}ESO (top) and C_{12}ESO (bottom) with various oils

Table 5. 1. PITs of CnESO with various oils various brine concentration

Surfactant	Oils	EACN	IFT_{min} (mN/m), 0 wt% Salt Microemulsion	PIT (°C)			
				Salt content (wt%)			
				0	1	5	10
C_{10}ESO	Cyclohexane	2.2[7]	$1.52*10^{-3}$	24	22	18	14
C_{10}ESO	Methylcyclohexane	3.2[8]	$2.29*10^{-3}$	30	28	24	15
C_{10}ESO	Ethylcyclohexane	3.8[9]	$2.26*10^{-3}$	44	42	34	28
C_{10}ESO	Propylcyclohexane	5.6[9]	$9.76*10^{-3}$	60	60	50	40
C_{12}ESO	n-Hexane	6 [7]	$9.73*10^{-4}$	20	18	16	10
C_{12}ESO	n-Heptane	7 [7]	$2.30*10^{-4}$	25	25	20	15
C_{12}ESO	n-Octane	8 [7]	$7.58*10^{-4}$	32	30	25	22
C_{12}ESO	n-Nonane	9 [7]	$3.21*10^{-4}$	38	35	31	30
C_{12}ESO	n-Decane	10 [7]	$5.58*10^{-4}$	45	45	40	30

5.4.2 HLD model parameters

By doing a simple linear regression of the EACN vs. PIT data in the absence of salt according to the equation 5.2., the parameters $^{c_T}/_K$ and $^{Cc}/_K$ were obtained from the slope and the intercept of the line respectively. These data are presented in Table 5.2. EACN vs. PIT of C_{10}ESO and C_{12}ESO in comparison with various alcohol ethoxylate surfactants by Sottman and Strey [4] are fitted with lines as presented in Figure 5.2. Both the sulfoxide surrfactants presented lower $^{c_T}/_K$ than AE

surfactants, which means the PITs are more sensitive to a change in EACN for the latter.

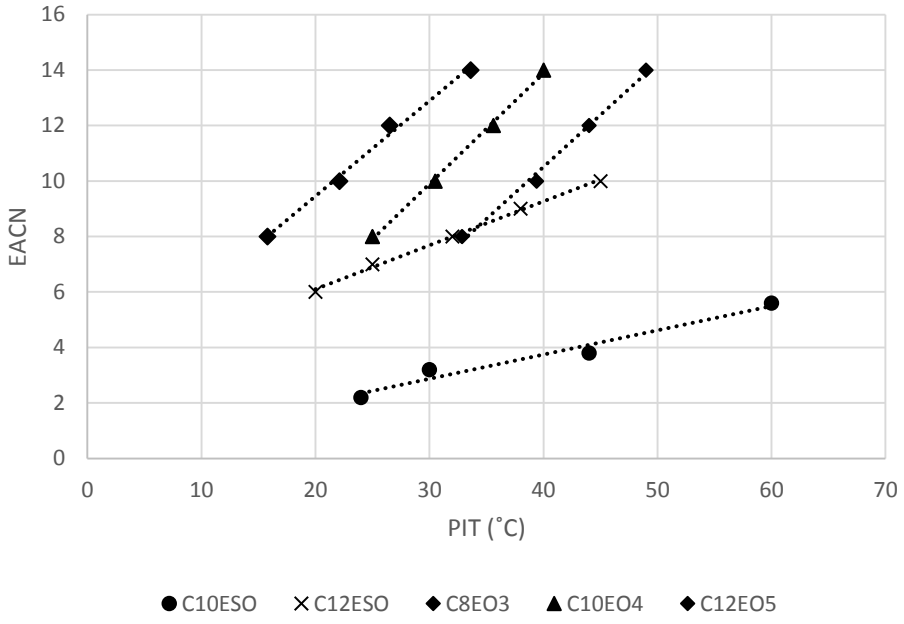

Figure 5. 2. EACN vs. PIT curves for C_{10}ESO and C_{12}ESO in comparison with various AE surfactants by Sottman and Strey

To find the four unknowns in Equation 1.27 for the ester sulfoxides, PITs of sixteen microemulsions of C_{10}ESO (four oils with four concentrations of brine) and twenty microemulsions of C_{12}ESO (five oils with four concentrations of brine) were found experimentally. The S values for each microemulsion were substituted in equation according to the concentration of the brine used.

Table 5. 2. HLD parameters of C_{10}ESO and C_{12}ESO compared with three AE surfactants [4]

Surfactants	$c_T/_K$	$Cc/_K$
C_{10}ESO	0.087	2.43
C_{12}ESO	0.16	6.89
C_8EO_3	0.34	11.17
$C_{10}EO_4$	0.39	7.90
$C_{12}EO_5$	0.37	4.89

EACNs of the oils used in each microemulsion and PITs ($\Delta T = PIT - 25$) were substituted in equation 1.27 accordingly while HLD was equated to zero. This resulted in a system of sixteen sets of homogeneous equations for C_{10}ESO surfactant and twenty sets of homogeneous equations for C_{12}ESO surfactant. The trivial solution (i.e. all adjustable parameters = 0) to sets of homogeneous equations obviously does not provide the ester sulfoxide parameters. The nontrivial solution could not be found for this system of equations since the coefficient matrix is not a singular matrix i.e. a solution to make all HLDs equations exactly equal to zero could not be found. Hence a numerical method instead of matrix method was used to solve for unknowns.

The K, Cc, C_T and b variables were varied in the ranges $0.1 < K < 0.3$, $-14 < Cc < 14$, $0 < c_T < 2$, $0 < b < 3$ accordingly and the absolute values of the all individual HLD equations were minimized simultaneously. The HLD parameters were

obtained such that the sum of absolute values of the HLD parameters were minimized.

Values for b, Cc, c_T and K were obtained and presented in Table 5.3. The Cc value of C_{12}ESO was found to be higher than that of C_{10}ESO which shows C_{12}ESO is more hydrophobic than the C_{10}ESO as expected. b was found to be 0.01 for C_{10}ESO and 0.02 for C_{12}ESO . K was found 0.10 for C_{10}ESO and 0.12 for C_{12}ESO surfactants. c_T was found to be 0.01 K^{-1} for C_{10}ESO and 0.02 K^{-1} for C_{12}ESO. We do not believe that the differences in any of these numbers between the two surfactants are statistically significant; error bars represent the error in the non-linear fits and we believe are an underestimation of the actual error. The value of the temperature coefficient is smaller than that reported for alcohol ethoxylates; c_T for AEs has been measured as 0.061 [4] and did not change with a change in aliphatic chain length. The value for the sulfoxide surfactants is equal to that typically found for ionic surfactants, although the temperature term is of opposite sign in the HLD equation for ionic surfactants as shown in Equations 1.26 and 1.27. In other words, in ionic surfactants the surfactant becomes more hydrophilic with temperature, while with nonionic surfactants, the surfactant becomes more hydrophobic with temperature.

Table 5. 3. c_T and Cc of C_{10}ESO and C_{12}ESO compared with three AE surfactants [4]

Surfactants	**c_T**	**Cc**	**b**	**k**
C_{10}ESO	0.01	0.24 ± 0.024	0.01 ± 0.002	0.10 ± 0.005
C_{12}ESO	0.02 ± 0.001	0.82 ± 0.057	0.02 ± 0.001	0.12 ± 0.008
C_8EO_3	0.061	1.9	-	0.1 - 0.2
$C_{10}EO_4$	0.063	1.4	-	0.1 - 0.2
$C_{12}EO_5$	0.061	0.87	-	0.1 - 0.2

Based on Cc, the indicator of surfactant hydrophobicity at 25˚C with no added salt, C_{12}ESO (Cc = 0.82) is almost equally hydrophobic to $C_{12}EO_5$ (Cc = 0.87) [4], indicating that 1 ester sulfoxide (ESO) unit is as essentially as hydrophilic as 5 EO groups. Since $C_{12}EO_6$ has a Cc of -0.2 [9], a linear interpolation for this one sample indicates that ESO is equivalent exactly to 4.90 EO groups. A similar comparison done between C_{10}ESO (Cc = 0.24) and $C_{10}EO_5$ (Cc = 0.1) [9], also shows that 1 ESO unit is essentially as hydrophilic as 5 EO groups. Linear interpolation with $C_{10}EO_4$ (Cc = 1.4) gives a value that ESO is equal to 4.87 EO groups.

References

[1] Viades-Trejo, J., Gracia-Fadrique, J., Colloid and Surfaces A: Physiochemical and Engineering Aspects, 302 (2007), 549-552.

[2] Vonnegut, B., Rev Sci Instrum, 13 (1942), 6-9.

[3] Huh, C., Journal of Colloid and Interface science, 71 (1979), 408-426.

[4] Sottmann, T., Strey,R, J Chem Phys, 106 (1997), 8606-8615.

[5] Marquez, N., Graciaa, A., Lachaise, J., Salager, J.L., Langmuir, 18 (2002), 6021-6024.

[6] Salager, J.L., Marquez, N., Graciaa, A, Lachaise, J., Langmuir, 16 (2000), 5534-5539.

[7] Bourrel, M., Schechter, R.S., Microemulsions and related systems: formulation, solvency and physical properties. 1988, New York: M. Dekker.

[8] Bouton, F.O., Durand, M., Nardello-Rataj, V., Borosy, A., Quellet, C., Aubry, J.M., Langmuir, 26 (2010), 7962-7970.

[9] Queste, S., Salager, J.L., Strey, R., Aubry, J.M., Journal of Colloid and Interface science, 312 (2007), 98-107.

6. Conclusions and recommendations

6.1 Conclusions

Sulfoxide-based nonionic surfactants derived from the reactions of fatty alcohols or fatty amines with 2-hydroxy-4-(methylthio) butyric acid were surface active. Surface tension reduction efficiency of a surfactant which is indicated by pC20 was measured to be 3.2 for C_8ESO compared to 5.8 for NPE9 and 5.3 for $C_{12}EO_7$. Surface tension reduction effectiveness of the surfactant which is indicated by γ_{CMC} was measured to be 29 mN/m for C_8ESO, 33 mN/m for NPE9 and 34 mN/m for $C_{12}EO_7$. Table 6.1 below shows the comparison of the cmc of the C_mE_n surfacatnts with ester sulfoxides. Ester sulfoxides nonionic surfactants have similar surface activity as of C_mE_n surfactants.

Table 6. 1. Comparison between the cmc of ester sulfoxides and C_mE_n surfactants

Surfactant	cmc (mM)
$C_{10}EO_4$	0.61
$C_{10}EO_5$	0.76
$C_{12}EO_5$	0.05
$C_{12}EO_6$	0.086
$C_{12}EO_7$	0.085
$C_{12}EO_8$	0.08
C_6ESO	104
C_8ESO	11.7
C_{10}ESO	0.59*

C_{12}ESO	0.06*

*: extrapolated from the CMCs of C8ESO and the mixtures. The pure materials were not water-soluble.

Unique properties, such as high cloud points, low surface tension at the CMC, and low surface area at the solution-air interface and fast adsorption kinetics were found. These surfactants have good wetting kinetics and in general their foams dissipate faster than a nonyl-phenol ethoxylate surfactant. For example C_8ESO foam dissipated approximately 5 times faster than NPE9. These surfactants were synergistic with sodium dodecyl sulfate at the same level with other nonionic surfactants as determined by surface tension measurements. In laundry testing, the performance of the formulation with C8/C12ESO-70 was on the average identical to the same formulation with a nonyl phenol ethoxylate surfactant.

Adsorption of the ester sulfoxide surfactant with one ester sulfoxide group attached to a C8 chain at the air/water interface is diffusion-controlled for dilute solution and 25°C. The Langmuir adsorption isotherm was satisfactory for describing the adsorption behavior.

Dynamic surface tension profiles obtained from the bubble pressure tensiometer were analyzed in terms of the asymptotic solutions of the Ward and Tordai equation. The DST data for different surfactant solution linearized when plotted vs $t^{1/2}$ and $t^{-1/2}$ suggested that the adsorption process is diffusion-controlled at short and long-times respectively. An average diffusion coefficient of (3.96 ±3.41) *

10^{-10} m^2/s obtained from the analysis of the bubble pressure DST data. To check whether the adsorption is diffusion-controlled over the entire time range the DST profiles obtained by the drop shape analyzer were compared with the prediction of the diffusion model over the time range of 5s-3000s. Using the Langmuir isotherm and varying the diffusion coefficient, agreement was obtained between the theoretical profiles and the experimental DST profiles of the shape analyzer. An average diffusivity of $(3 \pm 0.45)*10^{-10}$ m^2/s was obtained from the analysis of the DST profile from the shape analyzer.

The average diffusion coefficient obtained from the analysis of the bubble pressure DST profiles was larger than the average diffusion coefficient obtained from the analysis of the shape analyzer DST profiles. The reason for such difference might be due to possible existence of convection in the bubble pressure tensiometer measurements.

The surfactant diffusivity can be estimated from the well-known Stokes-Einstein Equation.

$$D_{AB} = \frac{K_B T}{6\pi R_A \mu_B} \tag{6.1}$$

Where D_{AB} is the diffusivity of the solute A in the bulk phase of solvent B, K_B is Boltzmann's constant, μ_B is the viscosity of the solvent, and R_A is the radius of the solute (assuming the solute is sphere): volume per molecule of solute = $\left(\frac{4}{3}\right)\pi R_A^3 = V_A/N_A$. Here V_A, is the molar volume ($=M_A/\rho_A$), M_A is the molecular weight, ρ_A is

the density of the liquid solute, and N_A is the Avogadro's number. The diffusivity of the C_8ESO was found to be $4.8*10^{-10}$ m^2/s at 25° C using Equation 6.1. The reason for discrepancy between the values obtained by the Stokes-Einstein equation and the experimental values might be due to the assumption of the surfactant molecules being sphere.

The results of the microemulsion study showed that optimum middle phase microemulsions were formed with sulfoxide based surfactants at PITs for all oils tested with and without the presence of electrolyte. PITs were screened with visual temperature scan of microemulsions and verified by IFT measurements. Ultralow water/oil IFT as low as 10^{-4} mN/m were obtained with these systems. PIT data were fitted to the semi-empirical HLD model to obtain ester sulfoxide HLD model parameters. These microemulsion studies indicate that one sulfoxide ester has about the same hydrophilicity as 5 EO groups. The temperature dependence for optimal microemulsions is approximately four times less for these ester sulfoxide surfactants compared to ethylene oxide surfactants, but, as with the latter, ester sulfoxide surfactants become more hydrophobic with an increase in temperature.

6.2 Recommendations for Future work

1) Determining the kinetic rate constants for adsorption/desorption at the liquid-air interface. In the re-equibiliration experiments when the interface is compressed or expanded from equilibrium the mechanism of the mass transport might be mixed-

controlled instead of diffusion-controlled and therefore the kinetic constants can be found from this experiment.

2) Measure the area per molecule of the surfactant at the cmc using neutron reflection to confirm the data obtained by tensiometry [2].

3) Thermodynamic of micellization and adsorption [3].

References

[1] Lin, SY., McKeigue, K., Maldarelli, C. Langmuir, 10 (1994), 3442-3448.

[2] Simister, EA., Thomas,RK., Penfold, J., Aveyard, R., Binks, BP., Cooper,P., Fletcher,PDI., Lu, JR. and Sokolowski, A. J. Phys. Chem. 96 (1992), 1383-1388.

[3] Al Sabagh, AM., Kandil, NGH., Badawi, AM., El-Sharkawy, H. Colloid and surfaces A: Phisiochemical and Engineering Aspects, 170 (2000), 127-136.